Empirical Thermal Performance Investigation of a Compact Lithium Ion Battery Module under Forced Convection Cooling

Akinlabi Akindimeji Abdul Hakeem

Submitted to the
Institute of Graduate Studies and Research
in partial fulfillment of the requirements for the degree of

Master of Science
in
Mechanical Engineering

Eastern Mediterranean University
January 2020
Gazimağusa, North Cyprus

Approval of the Institute of Graduate Studies and Research

Prof. Dr. Ali Hakan Ulusoy
Director

I certify that this thesis satisfies all the requirements as a thesis for the degree of Master of Science in Mechanical Engineering.

Prof. Dr. Hasan Hacışevki
Chair, Department of Mechanical Engineering

We certify that we have read this thesis and that in our opinion it is fully adequate in scope and quality as a thesis for the degree of Master of Science in Mechanical Engineering.

Asst. Prof. Dr. Davut Solyalı
Supervisor

Examining Committee

1. Assoc. Prof. Dr. Qasim Zeeshan

2. Asst. Prof. Dr. Davut Solyalı

3. Asst. Prof. Dr. Mehmet Şenol

ABSTRACT

Lithium ion Batteries (LIBs) are considered one of the most suitable power options for Electric Vehicle (EV) drivetrain, are known for having low self-discharging properties hence provide long life cycle operation. To obtain maximum power output from LiBs, it is necessary to critically monitor their operating conditions. Temperature particularly, is known to directly affect the performance and life span of LiBs. This paper investigates the performance of a Battery Thermal Management Systems (BTMS) for a battery pack that houses 100 Nickel Cobalt Rechargeable 18650 (NCR18650) Lithium ion cells built as part of an electric vehicle racing development process. Thermal performance of the battery pack is investigated under three levels (1.4, 2.4 and 3.4 m/s) of air flow rate and two current rate (0.5 and 0.75C). A worst case scenario of averaged maximum cell temperature of 36.1 °C was recorded during a 0.75 C charge experiment and 37.5 °C 0.75 C discharge under the least flow rate. A reduction in maximum temperature difference of 54.28% by increasing the air flow rate in a 0.75 C charge experiment to 3.4m/s was achieved. Increasing performance with increasing airflow rate was a common trend observed in the experimental data after analyzing various experiment results. A model for the investigated battery pack was developed by training an Artificial Neural Network (ANN) utilizing the Bayesian Regularization algorithm. An R-Value of the regression plot of the overall trained model of 0.988 was achieved. The model was tested and able to predict maximum temperature values with a maximum percentage error of 10.38% for the given input data from the experiments performed.

Keywords: Air-Cooled BTMS, Compact Lithium Ion Battery Module, ANN, RSM.

ÖZ

Lityum iyon piller (LIB'ler), Elektrikli Araç (EV) aktarma organları için en uygun güç seçeneklerinden biri olarak kabul edilir, düşük kendi kendine deşarj özelliklerine sahip olduğu için bilinir, böylece uzun ömürlü çalışma sağlar. LiB'lerden maksimum güç çıkışı elde etmek için, çalışma koşullarını eleştirel olarak izlemek gerekir. Özellikle sıcaklığın LiB'lerin performansını ve ömrünü doğrudan etkilediği bilinmektedir. Bu makalede, elektrikli araç yarışları geliştirme sürecinin bir parçası olarak inşa edilmiş 100 NCR18650 Lityum iyon hücresi barındıran bir pil takımı için BTMS'nin performansı araştırılmaktadır. Pilin termal performansı, üç seviye (1.4 m/s, 2.4 m/s ve 3.4 m/s) hava akış hızı ve iki akım hızı (0.5 C ve 0.75 C) altında incelenir. 36.1 °C 'de ortalama maksimum hücre sıcaklığının en kötü senaryosu, bir 0.75C şarj deneyi ve 37.5 °C 0.75 C deşarjı sırasında en düşük akış hızı altında kaydedildi. 0.75C şarj deneyinde hava akış hızını 3.4m / s'ye yükselterek maksimum sıcaklık farkında% 54.28'lik bir azalma sağlandı. Artan hava akış hızı ile artan performans, çeşitli deney sonuçlarını analiz ettikten sonra deneysel verilerde gözlenen yaygın bir eğilimdi. Bayesian Düzenleme algoritması kullanılarak bir sinir ağı eğitilerek araştırılan pil paketi için bir model geliştirilmiştir. Toplam eğitilmiş 0.988 modelinin regresyon grafiğinin R-Değeri elde edildi. Model test edildi ve yapılan deneylerden verilen girdi verileri için maksimum% 10.38 hata yüzdesi ile maksimum sıcaklık değerlerini tahmin edebildi.

Anahtar Kelimeler: Hava Soğutmalı BTMS, Kompakt Lityum İyon Pil Modülü, YSA, RSM.

To My Family

ACKNOWLEDGMENTS

It is my honor and privilege to sincerely acknowledge my supervisor Asst. Prof. Dr. Davut Solyalı for his support, guidance and great patience in assisting me throughout the entire period of my thesis. I also thank Him most importantly for the knowledge and exposure he gave me while working at the EMU EVDC laboratory. Also special thanks and deep appreciation to my friends Amir, Parsa Kolah Kaj, Hatim Shams and other colleagues in the EMU EVDC Laboratory that enabled me carry out my study in any way possible.

A very Special thanks and appreciation to Assoc. Prof. Dr. Qasim Zeeshan for the countless hours of counseling, motivation and guidance He provided me as a tutor and as a father.

Special thanks to the entire academic staff of the mechanical engineering department for making the department a conducive and friendly place that enabled me carry out my academic duties in my best state of mind.

To my colleagues and friends; Mohammed Alibar Yasin, Omer Kalef, Abubakar Abdusalaam Nuhu, Mr. Fubara Otonye, Hatim Shams and Tauqir Nasir, I thank you all for being there along the way.

Lastly, my deepest appreciation goes to my Parents back at home for not allowing me to quit when things seemed impossible.

TABLE OF CONTENTS

LIST OF TABLES

LIST OF FIGURES

LIST OF SYMBOLS AND ABBREVIATIONS

°C	Degree Celsius
A	Ampere
Ah	Ampere Hour
Ah	Ampere Hour
ANN	Artificial Neural Network
BM	Battery Module
BMS	Battery Management Systems
BP	Battery Pack
BTMS	Battery Thermal Management Systems
C	Capacity
CC-CV	Constant Current – Constant Voltage
CFD	Computational Fluid Dynamics
DoE	Design of Experiment
EA	Electro Automatik
EMF	Electromotive Force
EV	Electric Vehicle
KW	Kilo-Watts
KWh	Kilo-Watts Hour
Li	Lithium
LiB	Lithium Ion Batteries
m/s	Meters per Second
MDF	Medium Fibre Board
MJ/KG	Mega-Joule per Kilogram

MOGA	Multi-Objective Genetic Algorithm
MSE	Mean Square Error
NCR	Nickel Cobalt Researchable
RMSE	Root Mean Square Error
RSM	Response Surface Model
SMPS	Switch Mode Power Supply
SOC	State of Charge
SOH	State of Health
SSE	Sum of Square Errors
T-DAQ	Temperature Data Acquisition System
T_{INC}	Temperature Increase
T_{MAX}	Maximum Temperature
V	Voltage
ΔT_{MAX}	Maximum Temperature Difference

Chapter 1

INTRODUCTION

1.1 The State of Lithium Ion Batteries for Electric Vehicles

The growing global concern of the causes and effects of climate change which has led to stricter environmental regulations on carbon based machines [1], [2], coupled with huge advancements in portable battery technology specifically lithium ion, Electric Vehicles (EVs) and hybrid Electric vehicles are starting to disrupt the automobile industry markets by presenting themselves as vehicle choice of the future [3]. Some major hindrances to electric vehicle mass adaptation are range anxiety of EVs, lack of super-fast charging, performance driving etc. [1], [4]. Performance driving and fast charging problems of EV are due to the limitation of lithium ion batteries to perform outside tight operating temperature ranges [5]. Range anxiety problem of electric vehicle is also attributed to the gravimetric density of Lithium ion Batteries (LiBs). When compared to traditional gasoline powered vehicles, the average Energy-to-Weight ratio of lithium ion batteries is 0.3MJ/Kg and over 30MJ/Kg for gasoline powered vehicles [6].

While the current gravimetric property limitation of LiBs may be a design constraint on EV performance, EV manufacturers have the freedom to design robust Battery Thermal Management Systems (BTMS) for EV Battery Packs (BP) to efficiently limit amount of heat generated by LiBs during their operating cycles (Charge/Discharge). As LiBs performance is closely affected by temperature during

operation, LiBs tend to pose safety issues, face performance drawdown issues [1] such as electrolyte decomposition at high temperatures [7], energy and battery power suppression at extremely low temperatures [8]. BTMS provides means of operating Li-ion battery packs under their nominal operating conditions. As Batteries will be the most expensive part in full-electric vehicles hindering their marketability [9], knowing factors that contribute to heat generation in LiBs and understanding their effects individually and in unison becomes upmost importance for EV manufactures to design robust control systems to manage Charge and Discharge cycle and efficient cooling systems. This in-depth knowledge is essential to enable EV manufacturers make intelligent tradeoffs between availability of cooling material, ease of application/implementation, maintenance, etc. which helps in bringing down cost of electric vehicles, and designing vehicles with highest reliability, lifetime and safety [4].

1.2 Structure of LiBs

In designing a BTMS to obtain the best performance from LiBs, understanding operational behavior and heat generation phenomenon of an individual Lithium ion cell is critical. Also, knowledge of their building components at the most basic level is important. There are three kinds of lithium ion cell configuration available in literature. They are; Cylindrical, Prismatic and Pouch cell configuration as presented in Figure 1.

Figure 1: Lithium Ion Cell Types [4]

Lithium ion cells are typically made by combining films of various components in a specific way that ensures the movement of freed electrons through and from a negative and positive electrode material when an Electromotive Force (EMF) is applied across the positive and negative current collectors of the cell. The application of an EMF across the negative electrode (anode) and a positive electrode (cathode) of a battery insights an electrochemical reaction inside the battery. This reaction is exothermic hence heat is generated and freed up lithium-ions (electrons) gives rise to electricity [10] as they move through layers of the cell i.e. cathode-separator-anode [11] and a connected load.

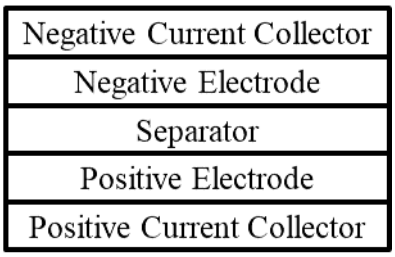

Figure 2: General Configuration of LiBs Adapted from [12]

Figure 2 shows a basic configuration of LiBs components which are generally wrapped into a cylindrical form to make cylindrical LiBs, or stacked to form prismatic or pouch cell type (see Figure 1) in a process called Lithium (Li) intercalation and Li insertion respectively [13]. In LiBs, the anode materials are always graphite which leaves the classification of LiBs based on the type of the cathode employed. A cathode in the cell can be one of these -*cathodes based on metal oxides, the cathode "spinel" and cathodes with transition metal phosphate*- [10]. During the charge cycle of LiBs, lithium ions move from cathode and are extracted to the anode while opposite scenario occurs during the discharge process [11]. Various Lithium ion batteries react differently to produce different number of

free Li electrons during their charge/discharge cycle. Table 1 shows various kinds of lithium ion batteries with their cathode chemical composition, their specific energies and typical application area.

Table 1: Chemical Composition of some LiBs [10], [14]–[16]

Cathode Type	**Cathode Chemical**	**Anode (Graphite)**	**Specific Energy (Wh/kg)**	**Self-Heating Temp (°C) at 100% SOC [Reference]**	**Application Area**
Lithium Cobalt Oxide (LCO)	$LiCoO_2$	Yes	150-200	131.5 [17]	Portable electronic devices
Lithium Manganese Oxide (LMO)	$LiMn_2O_4$	Yes	100-150	104.9 [18]	Medical devices, Electrical drive units
Lithium Nickel Cobalt Aluminum Oxide (NCA)	$LiNiCoAl_2$	Yes	200-260	84 [19]	
Lithium Iron Phosphate (LFP)	$LiFePO_4$	Yes	90-120	90 [16]	Portable application with high charge rate requirements
Lithium Titanate (LTO)	$Li_4Ti_5O_{12}$	Yes	70-80	-	Electrical drive units

1.3 Operating Lithium Ion Batteries: Thermal Constraints

Temperature rise as a result of heat generation from Joule effect and exothermic electrochemical reactions inside LiB are arguably the most important factor that affect the overall performance of LiBs and safety ([10], [20]). The aforementioned heat sources rely on the battery resistive phenomena which are; *the electric resistance inherent to the components (an ohmic resistance), the resistance related to the diffusion phenomena of Li+ through the different components of the cell (electrochemical resistance)* and *the resistance to the charge transfer at the interface*

between the solution and the insertion material (electrochemical resistance) [10], [20].

For the most popular cylindrical LIB used in most EVs (i.e., Panasonic 18650), their performance degrades as their operating temperature increases beyond the recommended optimal range, that is, batteries performing at temperatures above 40 °C suffers from critical battery capacity loss hence performance degradation, thermal runaway etc. [21] occurs. And performance also drops drastically at operating temperatures below 15 °C [22]. Figure 3 shows a graphical illustration of what operating temperatures above and below temperature limit causes and their effects on battery.

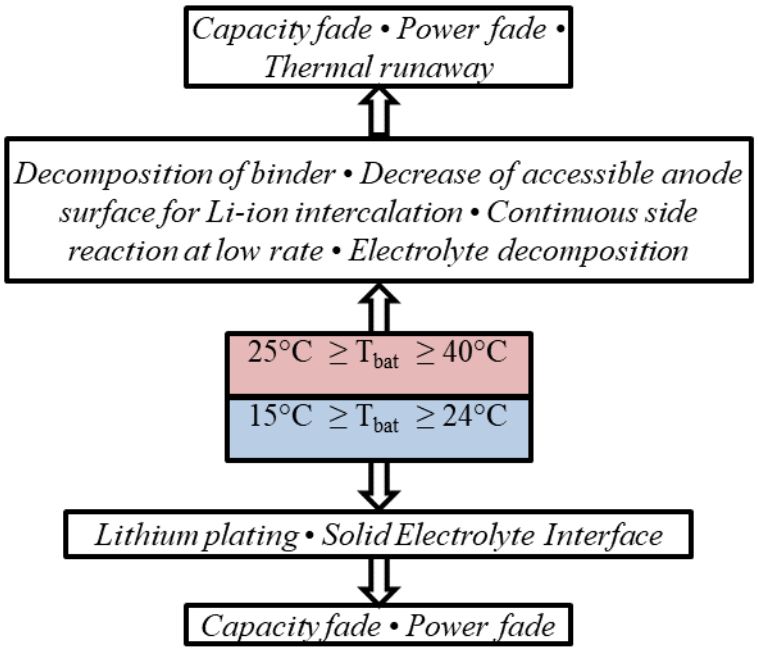

Figure 3: Causes and Effects of Battery Operating Temperatures on Cell Performance Adapted from [3], [9]

Once heat is generated in a cell, it is important to effectively dissipate the heat through transfer mediums to the surrounding environment. This could be done via

convection where heat is carried away from the battery by air, a non-conductive liquid medium [23], or via conduction where cells in a BP are in direct contact with a more conductive material (heat pipes) that channel the heat away from the battery pack [24], [25].

Knowing that cooling of battery packs depends on temperature of a heat sink (ambient) having significantly lower temperatures than that of the BP, therefore ambient conditions of where batteries are operated should be considered when designing a BTMS to efficiently perform cooling and to understand thermal behavior of an operating battery pack [11]. In absence of an efficient cooling strategy of a BP, heat generation inside the battery pack leads to heat accumulation which raises the overall operating temperature and this increases the maximum cell temperature difference between cells above allowable limits of 5 °C. The maximum allowable temperature between cells in a BP of 5 °C has been reported in several studies including [21], [26], [27] and [28], in order to promote battery balancing and uniform charging and discharging during the LiBs operating cycle. In extreme cases of heat accumulation, thermal runaway can occur, resulting in leaks, smoke, gas venting, flames, etc., which results in extreme safety hazards such as explosion and gas poisoning [16]. Thermal runaway is a concept of battery self-heating when several exothermic reactions occur inside a cell at extreme temperatures. Occurrence is independent of whether the battery is in use or not [16]. Table 1 shows various temperatures at 100% State of Charge (SOC) level at which thermal runaway occurs in some listed LiBs.

1.4 Battery Thermal Management Systems

Two main topics of concern in a BTMS are controlling the charge/discharge cycle of a BP, preheating of cells in a BP [29] and managing the high temperatures that arises from battery operation. Usually, the latter is encapsulated in the former, as temperature has a massive impact on the lifetime performance of all lithium-ion-based battery technology [25]. A BTMS serves as a temporary continuous means of improvement in the battery safety, performance, and lifespan of batteries in EVs. A lifespan of 10–15 years is a necessary requirement for LiBs that are targeted for EVs [30].

While the EV industry awaits for a major breakthrough in battery technology, such as a higher electrochemical potential per mass of a cell (specific energy) in a current battery technology [31], improving the volumetric and gravimetric densities for energy storage [32], or an absolutely new battery technology with overall improvement in performance, the current calendar life, safety, specific energy, and cost per power of existing battery technology depends on improvements of various BTMS in EVs.

1.5 Aim and Scope of Study

After establishing the fact about the reliance of EV on an effective BTMS, a detailed literature review will be carried out to identify various ways BTMS for EV are been improved by researchers in academia and in the industry. Various topics concerning air cooled BTMS for EV such as battery pack design improvement methods, ease of implementation and overall cooling performance will be sought out for during a literature review. Both physical experiment and simulation experiment study regarding air cooled BTMS will be investigated.

The aim of the study is to review various designs of air cooled BTMS, their key design variables and how they are optimized to obtain the most efficient BTMS methods through a comprehensive literature review. Achieving the later stated goal will then enable an original study to be carried out for this thesis in the following steps:

- *Study various BTMS model from literature to investigate their performance as stated in a published referenced study.*
- *Perform cooling experiment on an existing battery module using knowledge from literature review to build a cooling configuration.*
- *Develop a model for the designed battery pack using empirical data obtained from testings.*

The scope of this study is limited to the temperature control (cooling) aspect of BTMS for a battery pack with cylindrical Panasonic NCR18650B lithium ion cells.

Chapter 2

LITERATURE REVIEW

2.1 Classification of BTMS

To maintain the optimal working conditions of EV battery packs, a BTMS is supposed to carry out main objectives of increasing the lifetime of lithium ion cells and maintaining acceptable battery performance over the battery life by, regulating temperature levels and distribution [25], provide insulation to prevent sudden temperature changes and ventilation to exhaust potential hazardous gases from the battery pack [33]. These functions are usually accomplished in ways listed below [31];

- Monitoring the battery health to determine the State of Charge (SOC), State of Health (SOH) and other battery information useful to an EV user.
- Operating the battery in a safe an efficient manner, i.e., well within the required operating temperature limits.

In addition, a BTMS should be compact, light, have low design and production costs, high reliability, easy maintenance, etc., in order to be applied in EVs [1], [34].

BTMS are exhaustively classified under three main operating conditions, namely, the power consumption of the BTMS, the working fluid employed as a cooling medium in the BTMS, and the arrangements of the components inside the BTMS [9]. A sub categorization of an air-cooled BTMS, as reviewed in this study, is shown in Figure 4. The magnitude of heat generated from a BP inside an EV dictates the size, design,

operation mode and cooling medium employed in the BTMS of that EV [34]. In the scope of this review, air-cooled BTMS methods and optimization techniques employed by various researchers on the air-cooled BTMS are extensively discussed. Figure 4 also shows a flow chart of various topics to be reviewed in the following sections of this study.

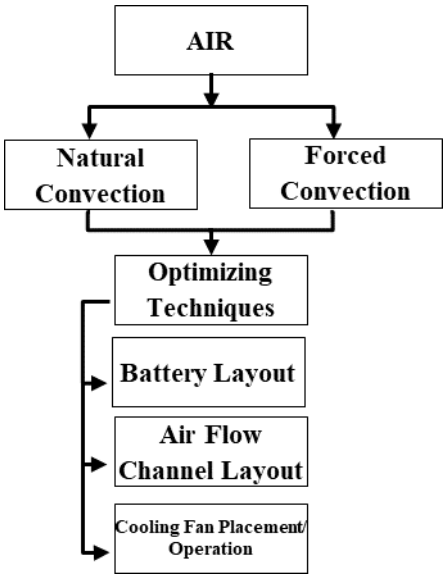

Figure 4: Classification of Air Cooled BTMS and Optimization Parameters Adapted from [1], [9].

2.1.1 Air Cooled BTMS

As the most traditional approach, air cooling has been studied intensively and is widely adopted in commercial applications [35]. An air-cooled BTMS is the simplest approach to tackling heat generation issues inside BPs and provides a solution when there are tight design space constraints inside an EV [36]. As categorized under natural and forced convection BTMS, the major difference between the two cooling strategies lies in their mode of operation.

2.1.2 Forced Convection BTMS

In this mode of the BTMS, forced air can be supplied to a BP from an additional fan option that is attached to a BP to limit extreme cases of temperature rise during extreme battery charge/discharge cases [9] as depicted in Figure 5 or by using pre-conditioned air from the vehicle air conditioning unit [3]. Wang et al. (2015) reported that for ambient air temperatures below 20 °C, forced air cooling is not needed for a BTMS [37]. In addition, cases where very high energy density cells are employed in BPs, forced air-cooling BTMSs are chosen over natural convection air cooling methods as convective heat transfer coefficient of passive air is much lower than that of forced air [35], [38].

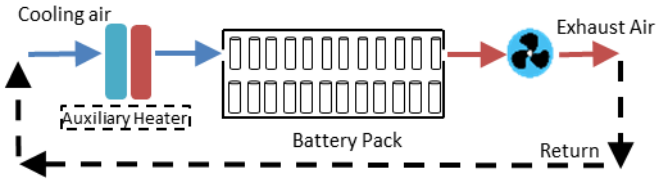

Figure 5: Forced Air Cooling BTMS Schematic Adapted from [39]

2.1.3 Natural Convection BTMS

In this mode of the BTMS, heat dissipation relies on continuous air flow channeled from outside a moving EV to a BP inside the EV. Heat generated from the BP is transferred to the ambient air by continuous flow of air generated by the vehicle's motion.

Relevant research to achieve better cooling performance can be classified into two fields, namely, optimizing battery layout and air flow configuration [40]. Here, the management system is completely void of any electronic device (see Figure 6), and thus a well-designed thermal management system that relies on natural convection is

used to achieve the objectives of the BTMS on the BP [41]. Improvements to the natural convection BTMS are mainly geometrical design optimization problems with multiple objectives, variables, and parameters [42], [43] and this concerns the design and optimization of the air flow channel in the BP.

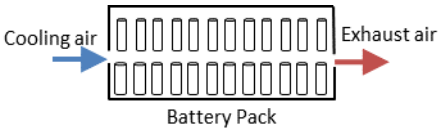

Figure 6: Natural Air Cooling BTMS Adapted from [10]

2.2 Trend of Study in Air Cooled BTMS

The importance of a BTMS, coupled with growing concern over reducing carbon fuel-based power systems in energy and transportation sectors, has allowed for a steady growth in BTMS as a research topic among academic scholars in the past decade in countries where carbon emissions is a major problem, such as China, the United States and Canada. Published documents from 2009–2018 regarding the BTMS have been gathered from the Scopus database presented in Figure 7. The results show a building momentum in the trend of research interest regarding the BTMS, specifically to those in EVs.

In Figure 7 series '*a*', each data point shows the number of published documents per year for topics specifically related to BTMSs and EVs from 2009 to 2018. No available documents were found pertaining to BTMSs and EVs from 2009 until 2011 when the first five documents were published. The statistic grew slowly until 2014, where 14 documents were published, and by 2018, 30 documents were published discussing BTMSs and EVs. While series '*a*' in Figure 7 shows the trend of research generally regarding BTMSs and EVs, series '*b*' and series '*c*' show newly

developing trends in research discussed in the scope of this review, and specifically concern applying optimization techniques to an air-cooled BTMS in an EV. A maximum of three documents was found from the Scopus database in 2017 in which the authors discussed applying optimization techniques to an air-cooled BTMS for an EV. In addition, data gathered from the Scopus database showed which countries are most active in the field of BTMSs and EVs. Figure 8 show that China has the most active research in the field of BTMSs and EVs. Fifty-one (51) documents regarding BTMSs and EVs have been published over the last decade from China, followed by the United States and Canada, with merely twenty (20) and nineteen (19) documents published, respectively, over the same time frame.

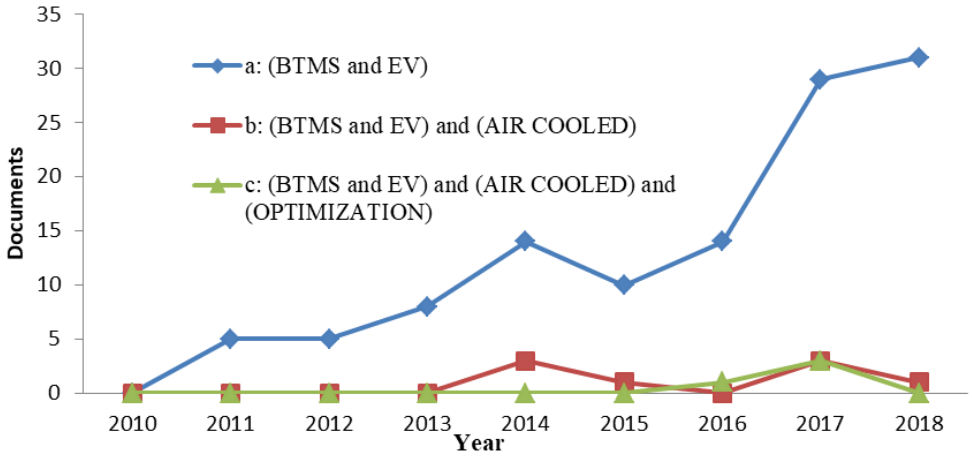

Figure 7: Statistics from Scopus Database in Published documents per year. Search keywords > series a: ((TITLE-ABS-KEY("Battery Thermal Management Systems" OR "BTMS") AND TITLE-ABS-KEY("Electric Vehicle" OR "EV")) AND PUBYEAR > 2009) series b: ((TITLE-ABS-KEY("Battery Thermal Management Systems" OR "BTMS") AND TITLE-ABS-KEY("Electric Vehicle" OR "EV")AND TITLE-ABS-KEY("Air Cooled")) AND PUBYEAR > 2009) series c: ((TITLE-ABS-KEY("Battery Thermal Management Systems" OR "BTMS") AND TITLE-ABS-KEY("Electric Vehicle" OR "EV") AND TITLE-ABS-KEY("Air Cooled") AND TITLE-ABS-KEY("Optimization")) AND PUBYEAR > 2009) [44]

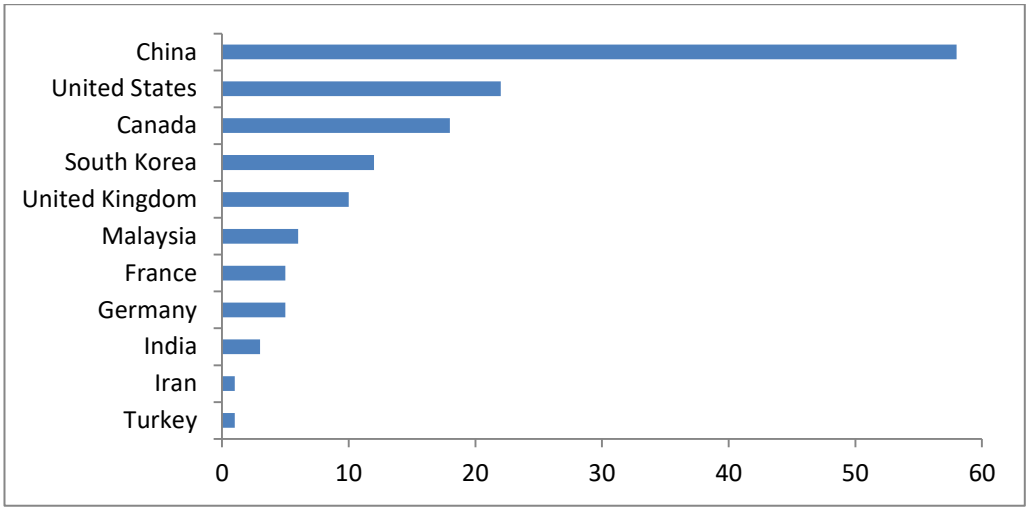

Figure 8: Statistics from Scopus Database in Published documents by country search keywords: ((TITLE-ABS-KEY("Battery Thermal Management Systems" OR "BTMS") AND TITLE-ABS-KEY("Electric Vehicle" OR "EV")) AND PUBYEAR > 2009) [44]

2.3 Related Works

There have been many studies performed in recent years to improve cooling performance by using techniques of optimizing the geometry of the air flow channel [1], the cell layout or the fan placement or operation. In this section, a detailed review of each technique found in literature is discussed, while the results and strengths of each method are highlighted.

2.3.1 Battery Layout Configuration

Various research studies have been conducted regarding improvements on cooling performance of this BTMS method, which deals primarily with design variables, pertaining to manners of arranging cells inside a BP to obtain the best performance. The most recent of them are discussed in the following paragraphs and typical performance results obtained by using this method in BTMS improvement, are summarized in Table 2.

Chen et al. (2017) performed a configuration optimization on prismatic lithium-ion cells for a parallel air-cooled system. In this model, the BTMS is optimized through arranging the spacing among the battery cells to obtain the best cooling performance. The optimization strategy is applied several times on a developed flow resistance model and a heat transfer model until the appropriate cell spacing is obtained. Their results exhibited a 42% reduction in the maximum cell temperature over their design variable optimization iterations on the developed model [45].

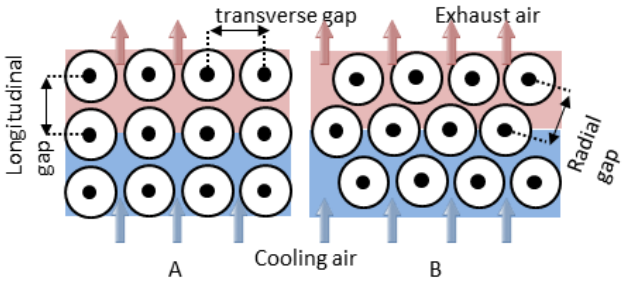

Figure 9: Schematic of Aligned (A) and Staggered (B) Cell Layout Optimization Adapted from [12]

By comparing an aligned versus staggered cell arrangement for a BTMS (see Figure 9 *A* and *B*), N. Yang et al. (2015) in [12] investigated the effects of transverse and longitudinal spacing between cylindrical cells in a BP with a forced-air cooling system. N. Yang et al. (2015) developed a numerical and thermal model for their BP, which was used in simulating various design variables. The model with the best performance results was then validated by physical experiment. N. Yang et al. (2018) reported that under a specific cooling air flow rate, the maximum cell temperature rise in a BP is proportional to the longitudinal interval for staggered arrays, whereas the inverse holds for aligned cell arrays. However, N. Yang et al. (2015) [12] provided results that proved that an increase in transverse cell distance has the same effect on the BP maximum temperature for both staggered and aligned cells. Finally,

they obtained a better performing BTMS model, by optimizing the longitudinal and transverse space between cells, coupled with optimizing an air inlet duct width for a BP with aligned arrangements [12]. Li et al. (2019) [46] proposed a BTMS method for a BP with prismatic cells, with a major focus on BP volume and cooling performance. Their BTMS investigation approach included modeling a BP module in a CFD simulation domain using ANSYS Fluent, applying a design of experiments (DoE) method in selecting design variables, developing and evaluating a surrogate model using variables and parameters selected by the DoE method and finally performing optimization on the surrogate model. A Multi-Objective Genetic Algorithm optimization (MOGA) was applied on their developed surrogate model to determine the optimal design variables (cell spacing distance) that produced the best cooling performance and the least BP volume [46]. They argued that their optimized model showed improvements in thermal performances. Liu et al. (2014) [47] investigated thermal behavior for a large BP with an air cooling system and examined the influence of the plate angle of the plenum and battery unit spacing on airflow and temperature distribution for a BP with a volume constraint. Part of their research objective was focused on designing a shortcut computational method of performing a thermal analysis on large BPs. They attributed the decrease in the temperature uniformity inside the BP to the wedge shaped plenum parameter [47]. After optimizing the model using the Runge-Kutta algorithm, a maximum temperature difference of 5 °C was achieved. They also argued that the modeling method can be used to conduct preliminary analysis and design of BPs [47]. Finally, Lu et al. (2018) provided a parametric study of forced-air cooling for lithium-ion batteries with staggered arrangements. They designed a three-dimensional simulation model (Gambit 2.4.6 CFD) of the BP that investigated the effects of cooling channel

size and air supply strategy for the model. The CFD model was solved using the Semi-Implicit Method for Pressure-linked Equations (SIMPLE) algorithm. They deduced that a cooling channel size of *1 mm* was appropriate for BPs with Panasonic 18650 cells. Furthermore, upon investigation, they reported the best cooling performance was achieved when placing the cooling air flow inlet and outlet on the top of the BP. Finally, they reported that the efficiency factor of a BTMS decreases with the number of cells in the horizontal direction; hence, they recommended a maximum of 10 cylindrical cells along the airflow direction for a BP [48].

2.3.2 Air Flow Channel Configuration

This method of improving BTMS cooling performance is observed to rely solely on selecting the best design variables for a BP that are related to the BP channel air duct. T. Yang et al. (2017) analyzed the thermal performance of axial flow air cooling for lithium-ion batteries to find the optimal radial distance between cells and the effect of air flux on the thermal performance of the cells. T. Yang et al. (2017) employed numerical methods coupled with a CFD program to develop a pseudo-two-dimensional model of 32 lithium-ion cells for a simulation experiment. Upon investigation, they reported that increasing the radial distances between cells resulted in a slight average temperature rise, but benefits the temperature uniformity of the BP. Secondly, they made the point that a larger radial interval significantly reduces the power cost of a cooling system; however, it causes a slight increase in volume of the BP. Lastly, regarding air flux, it was argued that a larger air flux in the battery pack is found to benefit the temperature uniformity within the BP [49]. Figure 10 presents the schematic of an axial air flow configuration, as studied by T. Yang et al. [49].

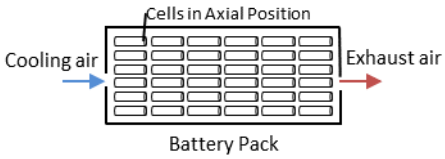

Figure 10: Battery Pack with Axial Cell Arrangement and Air Flow Adapted from [49]

R. Mahamud et al. (2011) [50], in a study to improve the lithium-ion cells' temperature uniformity in a BP for an EV, investigated a method of using a reciprocating air flow path in the BP, as presented in Figure 11. They employed a two-dimensional CFD model, and a lumped-capacitance model of their BP module and air flow network. Their numerical model results suggested that reciprocating air flow can reduce the cell temperature difference of the BP by approximately 4 °C (72% reduction) and the maximum cell temperature by 1.5 °C for a reciprocation period of 120 sec as compared with the unidirectional flow case [50]. A study similar to the one performed by R. Mahamud (2011) was presented by S. Wang et al. (2019) in [27], where the effect of reciprocating air flow on large Lithium NiMnCoO2 (NCM) pouch lithium-ion cells was investigated. S. Wang et al. achieved better cooling performance results for their battery module and concluded that the temperature non-uniformity caused by heat concentration and accumulation was greatly reduced by the reciprocating cooling air-flow path, along with optimizing a reversing time strategy based on the battery depth of discharge. S. Wang et al. (2019) in [27] also noted that maximum temperature of battery cells cannot be improved by relying only on reciprocating airflow. A different method of exploring an air flow channel for obtaining better cooling performance was presented in [51]. Na Kang et al. in [51] proposed a novel method of a reverse-layered air flow channel by partitioning the cell transversely within the BP. Their method, when compared with a unidirectional air flow channel in a three-

dimensional CFD environment, showed a 47.6% reduction in the maximum average temperature difference between the cells. Furthermore, they conducted optimization on their BTMS module, by adding rectifier grids to reduce temperature fluctuations at cooling air entrance of the battery pack, and altering cooling air velocities and cell distances in the BP to obtain optimal results [51]. Sun et al. (2014) [52] applied an analytical DoE method to develop an optimal cooling strategy for an air-cooled BTMS with pouch-style lithium-ion batteries. In their study, a three-dimensional BP thermal model with a "Z-type" air flow channel (Figure 12 *A*) was developed based on a simplified electrode theory. After that, they applied an optimal Latin-hypercube technique by incorporating a DoE design model into the correlated BP thermal model and performed optimization via a morphing model. Further studies by Sun et al. (2014) examined the effects of cooling duct geometry, cooling plates, etc. to obtain the best optimal cell conditions in the BP. They reported a maximum cell temperature and temperature difference between cells of 50 °C and 8.0 °C, respectively [52]. Similarly, Chen (2018) developed a numerical model for optimizing thermal management of a BP with a "U-type" flow (Figure 12 *B*). Based on a developed flow resistance model of the BP, the angles of the plenums and the widths of the air duct inlet and outlets were optimized using a nested looped procedure and numerical method.

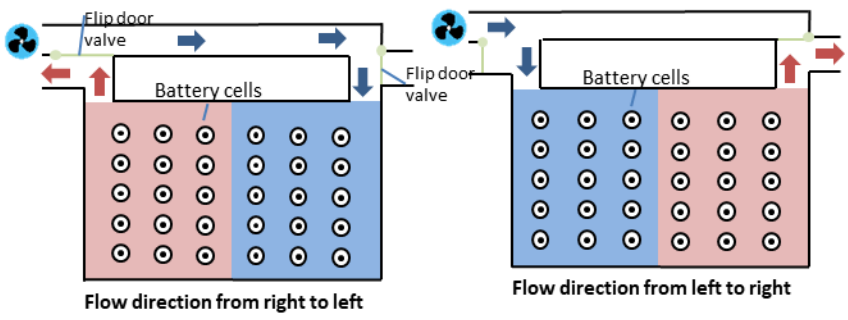

Figure 11: Reciprocating Series Cooling Air Flow BP adapted from [50]

The study was performed on twenty-four (24) lithium-ion prismatic cells investigated under two battery discharge conditions. The results after optimization showed a 70% reduction in cell temperature difference and a 32% reduction in the power consumed by cooling fans when compared to an un-optimized version of the flow model. They also argued that the main design factor that requires optimization to improve the efficiency of a BTMS is the width of the inlet and outlet air ducts on their model [53].

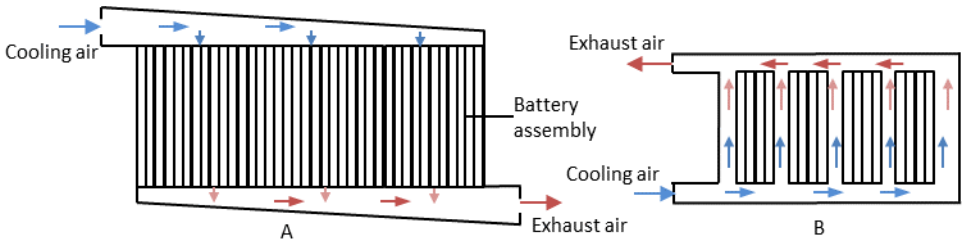

Figure 12: Z-type Parallel Air Flow (A) adapted from [52] and U-type Air Flow (B) adapted from [54]

An assessment on the air duct angle optimization by Chen et al. (2018) [53]was similar to the results of a study conducted by Xie et al. (2017) in [55], where a structural optimization of a BP with a forced-air cooling system was conducted. Xie et al. (2017) examined the influences of three factors, namely the air-inlet angle, air-outlet angle, and the width of the air flow channel between battery cells, on the efficiency in the BTMS. Simulation experiments (CFD) and physical experimentation were simultaneously employed by Xie et al. (2017) while investigating and optimizing their three design variables. A DoE method (single factor analysis and orthogonal test method) was applied on the set of design variables [55]. Xie et al. emphasized that the layout of an air flow channel has great impact on the BTMS objective function, and that the best cooling performance was obtained while optimizing the air duct inlet and outlet angles for equal channel width [55].

Their optimization method resulted in 12.82% and 29.72% improvements of the highest cell temperature and temperature difference between cells, respectively, when compared to the un-optimized models.

Table 3 summarizes various research conducted concerning improving a BTMS, via air flow channel configuration optimization, highlighting temperature results of various battery modules and other objective functions, design variables, simulation platforms, thermo-fluid models, etc.

A less observed approach to improving forced-air BTMS performance is by introducing a mixing and turbulence air flow inside a BP with axial air flow, as presented Shahid et al. (2018) [56]. A simulation (CFD) experiment was used to investigate a BP modeled with a secondary inlet that changes the direction of air flow and eliminates the problem of recirculation and non-availability of air between adjacent cells. Three models were investigated numerically and the most efficient model was validated experimentally with a single model. Their results showed 4% and 39% improvements in maximum cell temperature and cell temperature difference respectively, after optimization [56]. A similar method of BP design was implemented by Lu et al. (2016) [57] for a densely-packed BP with 252 lithium-ion cylindrical cells, whereas Hong et al. (2018) [58] studied the same module for a densely-packed prismatic cell. The numerical model in Lu et al. (2016) [57]examined the effects of multiple air outlet vents with various cooling channel widths.

2.3.3 Fan Placement or Operation Configuration

A sub-category method of improving cooling performance of a BTMS relates to optimizing the air flow channel as a major design variable, and can be observed when researchers focus on air flow design variables, in terms of minimizing fan

power consumption used for cooling and finding the most effective location to place inlet and outlet air vents on a BP to obtain maximum cooling performance. Various methods of this optimization strategy are discussed below, and summarized in Table 3.

Jiaqiang et al. (2018) in [59] designed a CFD method and a lumped thermal model for 60 cylindrical cells, to study the effects of the relative positions of airflow inlets and outlets on the cooling performance of a BP, as shown, e.g., in Figure 13. They introduced and investigated the effects of air baffle plates on cooling performance in a BP. They indicated that the cooling performances of models with air cooling vents on different sides are better than those of models having air cooling vents on the same side. The air baffles also had positive effects on the thermal performance [59]. A fan operation optimization technique applied to a BTMS was presented in T. Wang et al. (2015) [37]**.**

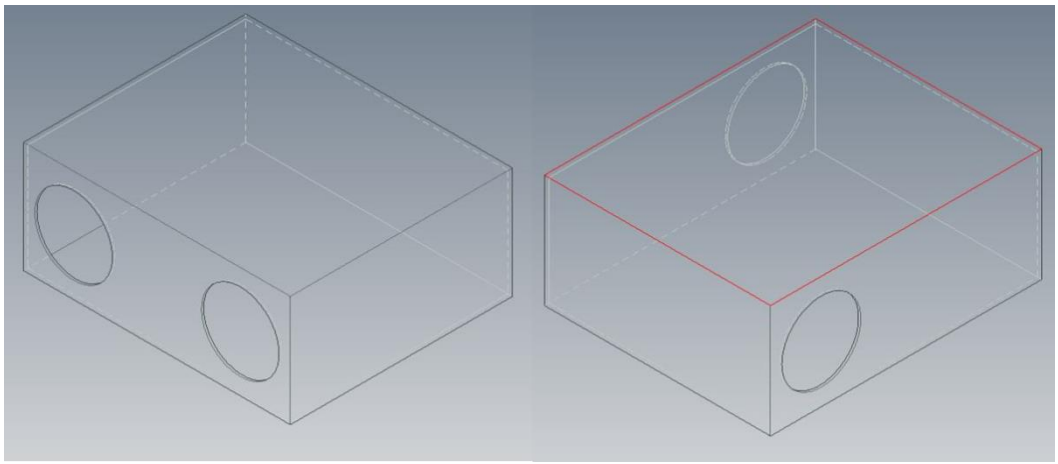

Figure 13: BP with Cooling Air Intake and Exhaust Vents on Different Sides adapted from [59]

The operations of cooling fans are optimized to operate at certain BP temperatures, to improve the BTMS power efficiency. The method was able to keep the BP

temperature within an acceptable operating temperature of lithium-ion cells for most discharge rates that were investigated, except for 5 C. Wang et al. (2015) in [37] revealed that the upper limit of the ambient temperature of forced-air cooling is 35 °C, and concluded that in a BP, forced-air cooling is not required when the ambient temperature is below 20 °C, except for during operations under high discharge rates [37]. Yu et al. (2014) in [60] investigated the effects on a BP of having two cooling air ducts with independent intake channels and fans. The separate air intake channels operated independently, with different functions. One fan operated for the purpose of cooling, whereas the second fan operated to improve air circulation inside the BP. A three-dimensional anisotropic heat transfer model was developed to perform simulation experiments to investigate the thermal performance of the model and a physical experiment was performed to validate the optimal simulation results. Their optimal model results were able to maintain the maximum cell temperature at 33.1 °C, and showed significant improvement in temperature uniformity inside the BP [60]. Yu et al. (2014) suggested that the two-directional air flow BTMS improves cooling efficiency, and that heat accumulation between middle cells in a BP can be greatly decreased through employment of a secondary fan [60].

2.3.4 Tabular Literature Review

In Table 2 and Table 3 is classification of more research work according to battery layout configuration and air channel configuration.

Table 2: Summary of Research on Battery Layout Configuration

Author [Ref]	BATTERY	Design Variables			OBECTIVES INVESTIGATED			SIMULATION				PHYSICAL EXPERIMENTS
	Num of Cells/ Capacity/ Discharge	Variables	Flow rate	$T_{Inlet\ Air}$ °C	T_{Max} °C	ΔT_{MAX} °C	Others	CFD	Meshing Elements/Type	Solver/ Thermo fluid Models	Platform/ Optimization Algorithm	
Li et al [41]	8 Prismatic	Cell Spacing	0.012 (kg/s)	-	-269	-273	-	CFD thermal & lumped Capacitance model investigation	34916	-	ANSYS, MATLAB/ MOGA	-
Jilte et al [61]	7 Cy Cells/-/ 9.4 & 11C	Cell Spacing	0.01, 0.05, 0.1 & 0.5 m/s	20, 25 & 30	Confined: 6.19°C < Opened	Confined 0.24°C < Opened	Pressure Drop, Pump power	CFD thermal model investigation	-	S.O.U.S	ANSYS FLUENT	One battery module in 1P*6S cell configuration was investigated to validate numerical model
Zhao et al [48]	14 Cy/ 2.2/ 0.5C	Cooling channel size, Air supply strategy	Laminar (Re < 2300)	20	30	10	Space utilization, Energy factor	CFD model, Analytical Thermal model investigation	1230858/ Structured Mesh	Green-Gauss node, S.I.M.P.L.E, etc.	ANSYS FLUENT	-

Author [Ref]	BATTERY	Design Variables			OBECTIVES INVESTIGATED			SIMULATION				PHYSICAL EXPERIMENTS
	Num of Cells/ Capacity/ Discharge	Variables	Flow rate	$T_{Inlet\ Air}$ °C	T_{Max} °C	ΔT_{MAX} °C	Others	CFD	Meshing Elements/Type	Solver/ Thermo fluid Models	Platform/ Optimization Algorithm	
Chen et al [45]	8 P/ 2.2/ 4&5C	Cell Spacing, Cooling air flow rate	.010, .012,.015,.018 (m^3/s)	27	54	3.5	-	Analytical FRN model, numerical CFD thermal model investigation	-	S.I.M.P.L.E/ K-Epsilon turbulence model [62], etc.	ANSYS FLUENT	-
N. Yang et al [12]	60 Cy/-/ 2C	-	2.5 m/s	5, 15 & 25	Staggered: 33.83, Aligned: 34.55	-	Power requirements, Cooling Index	1D electrochemical model investigation	-	/K-Epsilon Model	COMSOL	-
Liu et al [63]	8 Cy/ 2.2/ 4&5C	Plenum angles, width & Cell Spacing	0.04 (m^3/s)	-	-	-	less Computational time	FRN model with transient heat transfer model for thermal investigation	1,720,000	-	COMSOL/ Runge-Kutta	-
Fan et al [64]	8 P/ 15Ah	Cell Spacing, Cooling air scheme, etc.	10.2, 20.4, 30.6, 40.6 m^3/h	27	3mm, 40.6m^3/h 4.73	-	Fan power	3D transient Thermal analysis	100000/ Hexahedral Mesh	-	ANSYS	Thermal Imaging test of battery pack to validate CFD results

Author [Ref]	BATTERY	Design Variables			OBECTIVES INVESTIGATED			SIMULATION				PHYSICAL EXPERIMENTS
	Num of Cells/ Capacity/ Discharge	Variables	Flow rate	$T_{Inlet\ Air}$ °C	T_{Max} °C	ΔT_{MAX} °C	Others	CFD	Meshing Elements/Type	Solver/ Thermo fluid Models	Platform/ Optimization Algorithm	
Park and Jung [65]	-	Cell spacing, Flow rate	Range: 0 – 1 (m/s)	25	-	-	Optimal cell spacing,	Parametric 1D thermal model of BP model using Finite Differential Method (FDM) [66]	-	-	-	Compared 1D thermal model with published experimental data from Forgez et al [47] for thermal model validation
Cho et al [67]	88	Ambient temperature, etc.	Max: 2800 rpm	5, 35	11.66	-	-	Transient numerical thermal model investigation	-	-	Simulink, Matlab	Compared simulation generated results to published experimental data
Reyes- Marambio et al [68]	30 and 25 Cy/ 2.3Ah/ 1,2&3C	Staggered vs. Aligned , Spatially isolated cells	0, 2.0 & 2.5 (m/s)	-	-	-	-	Fractal time thermal modeling to predict surface temperature of Li-Ion cells	-	-	Wolfram Mathema-tica [68]	Built physical module of simulated battery packs for simulation results validation

Table 3: Summary of Research on Air Channel Configuration

Author [Ref]	BATTERY	DESIGN VARIABLES			OBECTIVES INVESTIGATED			SIMULATION				PHYSICAL EXPERIMENTS
	Num of Cells/ Capacity/ Discharge	Variables	Flow rate	$T_{Inlet\ Air}$ °C	T_{Max} °C	ΔT_{MAX} °C	Others	CFD	Meshing Elements/Type	Solver/ Thermo fluid Models	Platforms/ Optimization Algorithm	
S. Wang et al [27]	-/ 37Ah/ 3C	flow channel thickness, flow rate	15 m^2/s	-	-	-	-	-	-	-	-	Infrared Imager to measure thermal performance
Chen et al [54]	24Pouch/ 2.2/ 5C	Cell spacing	0.01, 0.012 & 0.015 (m^3/s)	27	54	1.3	-	Grid dependent CFD for thermal analysis, FRN for flow analysis	-	-	ANSYS/ Custom built	Aluminum blocks with heating elements as dummy batteries to validate CFD model
Shahid et al[56]	32 Cylindrical/ 2.5/ 1&2C	-	2.0, 2.2 & 2.8 (m/s)	23	3.4	9	BP Volume, Power Consumption	CFD and thermal investigation of BP model	8.2 million/ Unstructured Mesh	/Shear Stress Transport (SST) model[69]–[71]	LabView, ANSYS	Thermal investigation of physical battery models to validate Numerical Results, Heat flux measurements
Na Kang et al [51]	20Cylindrical/-/ 3C	Rectifier, air flow velocity, Cell spacing	1, 2, 3 (m/s)	-	38.2(with rectifier)	4.5 (without rectifier)	-	CFD Flow and Temperature field investigation	-	-	CATIA, ANSYS Fluent	Analogue BP model: 20 heating rods and AC transformer

Author [Ref]	BATTERY	DESIGN VARIABLES			OBECTIVES INVESTIGATED			SIMULATION				PHYSICAL EXPERIMENTS
	Num of Cells/ Capacity/ Discharge	Variables	Flow rate	$T_{Inlet\ Air}$ °C	T_{Max} °C	ΔT_{MAX} °C	Others	CFD	Meshing Elements/Type	Solver/ Thermo fluid Models	Platforms/ Optimization Algorithm	
Hong et al [58]	-/ 2.2/ 5C	-	0.01, 0.012, 0.015, 0.020 (m^3/s)	27	41	-	-	Grid dependent 2D CFD for thermal analysis	2.3 million grid number	S.I.M.P.L.E	ANSYS FLUENT	-
Xie et al [55]	10 Cylindrical/ -/ 20Ah	inlet and outlet angles, channel width	3 (m/s)	25	34.45	4.47	-	CFD Flow and Temperature field investigation	550000/ Hexahedral Mesh	S.I.M.P.L.E	ANSYS FLUENT	Test rig to validate CFD results for optimized parameters
Z. Lu et al [57]	252 Cylindrical	15 and 59 vented flow paths	Reynolds number < 2300	-	36.85	-	-	CFD model and Thermal resistance model	-	S.I.M.P.L.E	ANSYS FLUENT	-
T. Yang et al [49]	8 Cylindrical/ 8/ 2C	radial interval between cells	0.87, 0.83 & 1.03 (m/s)	25	-	-	Space efficiency, Power cost	CFD thermal and electro chemical model investigation	Fluid Zone: 2205939 solid zone: 92392	-	ANSYS FLUENT	Carried out a single cell thermal investigation to validate numerical models

Author [Ref]	BATTERY	DESIGN VARIABLES			OBECTIVES INVESTIGATED			SIMULATION				PHYSICAL EXPERIMENTS
	Num of Cells/ Capacity/ Discharge	Variables	Flow rate	$T_{Inlet\ Air}$ °C	T_{Max} °C	ΔT_{MAX} °C	Others	CFD	Meshing Elements/Type	Solver/ Thermo fluid Models	Platforms/ Optimization Algorithm	
Saw et al [72]	24 Cylindrical/ 8	Cooling air rate	5, 40, 75 (g/s)	30	33	1.5	-	CFD and thermal model analysis	58,511,496/ Hybrid Mesh	/SST Turbulence Model	ANSYS FLUENT	Thermal investigation of actual BP model to validate CFD results
Sun et al [52]	80 Prismatic	Cooling duct geometry, cooling channel size,	0.0283 m3/s	50	8	1.1	Pressure drop	De-Coupled 3D transient thermal model a 3D BP flow sub model and 1D BP network model investigation	-	/SST K-Omega Model	ANSYS, iSight Design, MATLAB	Model baseline test of battery pack to validate thermal models
R. Mahamud et al [50]	8 Cylindrical/ 3.5/ 7C	-	-	20	28.1 (averaged)	1.5	-	CFD and thermal model , Lumped Capacitance model analysis, etc.	113,470/ Quadrilateral Mesh	S.O.U.S, PISO, PRESTO	ANSYS FLUENT	BP thermal model investigation by in-line tube bank system
Jiaqiang et al [59]	60 Cylindrical/ 2.6/ 0.5&1C	Vent Position on BP	2 (m/s)	25	38.9	7.3	-	Lumped thermal model and CFD transient investigation	1,123,360/ O-grid elements	Navier-Stokes/ K-Epsilon Model	ANSYS FLUENT	Validation of thermal models, Determination of Cell entropy Coefficient, etc.

Author [Ref]	BATTERY	DESIGN VARIABLES			OBECTIVES INVESTIGATED			SIMULATION				PHYSICAL EXPERIMENTS
	Num of Cells/ Capacity/ Discharge	Variables	Flow rate	$T_{Inlet\ Air}$ °C	T_{Max} °C	ΔT_{MAX} °C	Others	CFD	Meshing Elements/Type	Solver/ Thermo fluid Models	Platforms/ Optimization Algorithm	
T. Wang et al [37]	5 Cylindrical/ -/ 1,2&3C	Fan Operation	1 & 2 (m/s)	20, 25, 30 & 35	-	-	BP temperature for forced air cooling	Empirical thermal method investigating a BP model	-	-	-	-
Yu et al [60]	-/ 180/ -	various air channel, jet holes	2300 (rpm)	24	33.1	1.2	-	3D transient thermal analysis profile for a BP model	3,000,000/ Structured Grid	S.O.U.S, Green-Gauss	ANSYS FLUENT	Investigated temperature rise in a BP with thermocouples
He et al [62]	-/ -/ 1.5C	Cooling air flow rate	CFD: 0.1 to 10 (m/s); Physical:0.5-30 (m/s)	18.7, 21.8	-	-	-	High fidelity 2D transient thermal analysis	189,852	Reynolds-Averaged Navier Stokes	ANSYS	Wind tunnel test on a BP module to validate CFD results

Chapter 3

INVESTIGATED DESIGN / METHODOLOGY

3.1 Preliminary Work

The battery module to be investigated in this thesis is based on a parent developed by the Eastern Mediterranean University (EMU) Electric Vehicle Development Centre (EVDC) as part of the international Turkish Efficiency Challenge [73], [74] . The battery module consist of Two-Hundred and Fifty-Two (252) NCR18560 (green) Li-ion cells connected in a 14S18P configuration (see Figure 14) to provide a total power capacity of 2.5Kwh minimum to cater for an electric vehicle with maximum speed of (60Km/h) during a race.

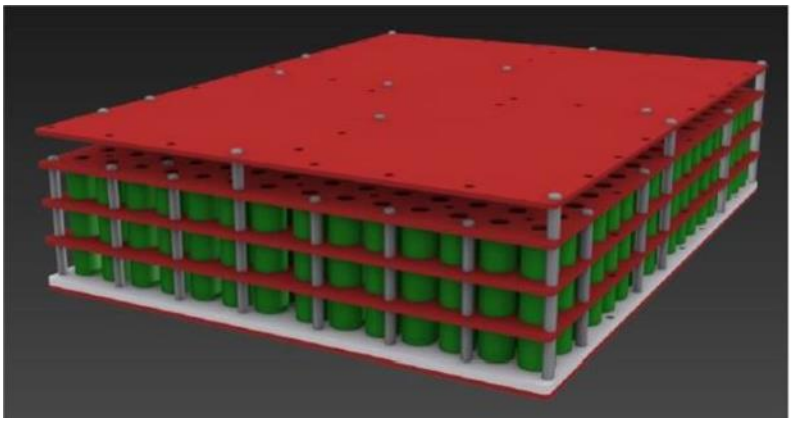

Figure 14: EMU Team ADA EVDC Battery Module

The cells in the battery module are arranged and enclosed in a tightly fashion to provide maximum rigidity, protection and ensure intact connections between the serial and parallel interconnections of the cells, by spot welded nickel strips (see Figure 15) during aggressive racing conditions.

Figure 15: Cell Connection inside Battery Pack

The casing for the battery module is designed and 3D printed in house consisted of six (6) layers of hard plastic (as seen in Figure 16 *b*) PCB FR4 material with eighteen (18) mm diameter cut outs as holding profiles for the cells (as seen in Figure 16 *a*). Layers of the housing are secured at heights with multiple stand-off screws which also serve an important role of providing rigidity for the battery module.

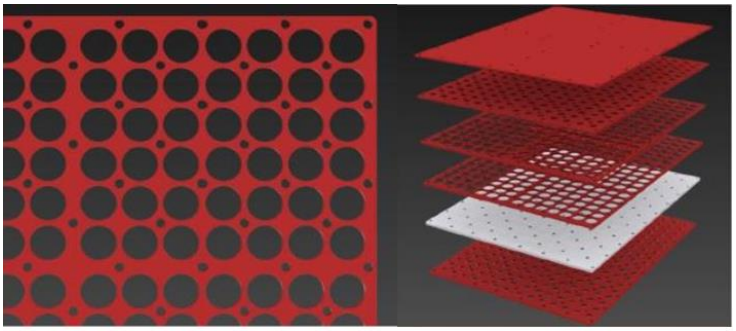

Figure 16: Battery Module Hole Profile and Housing Layers

The top most layer of the casing serves as a circuit board of the battery module for various electrical connections such as: temperature sensors placed in between multiple levels of the casing and the Battery Management System (BMS) circuitry. Figure 17 below shows the temperature sensors and the BMS circuitry connectors of the battery module.

Figure 17: Temperature and BMS Circuitry Connector Outlet

3.1.1 Battery Cooling Configuration

The battery module used by the EMU EVDC team ADA was cooled by a passive/active air BTMS. An outer casing made out of aluminum was designed and manufactured in house by the team. It featured four vents, one at each side of the battery case with the inlet vents slightly bigger at 80 mm while outlet vent were at 60mm. The battery case was positioned vertically at the front of the racing vehicle built and secured via mounting clamps constructed as part of the case and bolted onto the rolling cage of the vehicle.

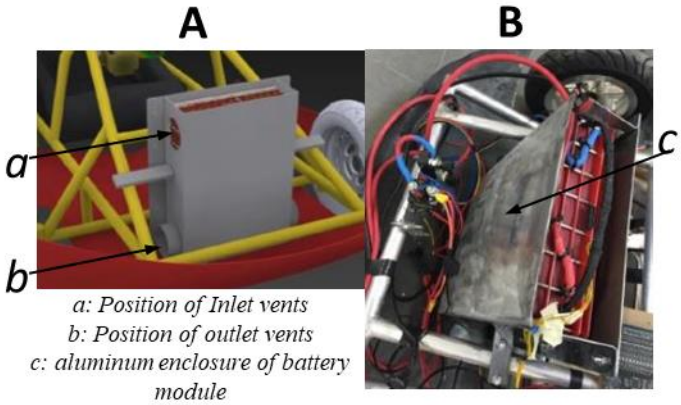

Figure 18: CAD Model of Battery Pack (A) and Real Life Implementation (B)

Figure 18 shows a pictorial representation of the original battery pack of which a similar design is studied in this thesis. Figure 18 “A” shows the battery pack at its design stage, while Figure 18 “B” shows its real life implementation.

To provide cooling air for the battery during vehicle operation, two connecting ducts were channeled from the front of the vehicle to the inlet vents of the battery case. Two cooling fans placed at the outlet vents operated passively to improve heat exhaustion from the battery pack during the vehicle operation while it operates actively when the vehicle is operating at a standstill.

3.2 Current work

In effort to obtain better performance from the discussed battery pack in Section 3.1 above, a smaller battery module of one hundred (100) cells (see Figure 19) pre built in a similar fashion as same as Figure 14 was tested.

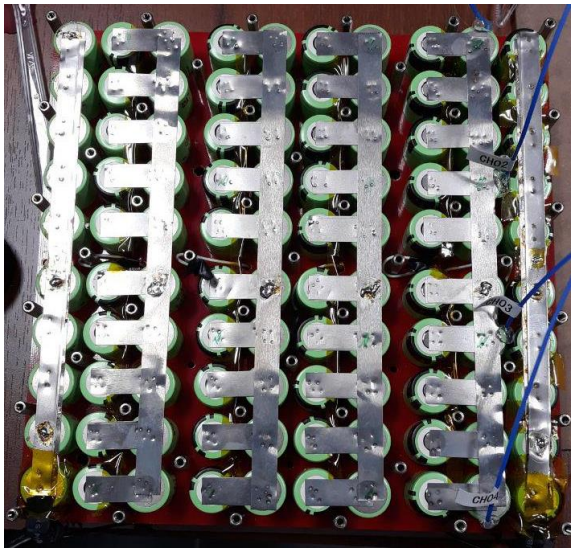

Figure 19: Battery Module Investigated

The cells in the battery module are connected in a 10 Serial and 10 parallel (10S10P) configuration to provide a power capacity of 1.024 KWh minimum and 1.344 KWh

maximum. Nominal data specification value of a single NCR18650 cell used in the battery module being tested are presented in Table 4 below.

Table 4: NCR18650B (Green) Specification [75]

Specifications	Value
Nominal Voltage	3.6 V
Cutoff Voltage	4.2 V
Minimum Rated Capacity	3.2 Ah

An experimental setup up was designed to test the battery module for real life scenarios while varying design variables such as; cooling air velocity and current flow rate of the battery pack.

The experimental setup in Figure 20 consists of a battery pack with four vent holes (two opposite ends) built from Medium Fiberboard (MDF), four switch mode power supply (SMPS) cooling fans, a 3D printed part connecting a flexible vent pipe to connect the fans to the atmosphere, a CPX400D power supply, a 16-channel Temperature Data Acquisition device (T-DAQ), a 4000W EA-EL 9200 electronic load and a 200V EA-PSI 9200 power supply.

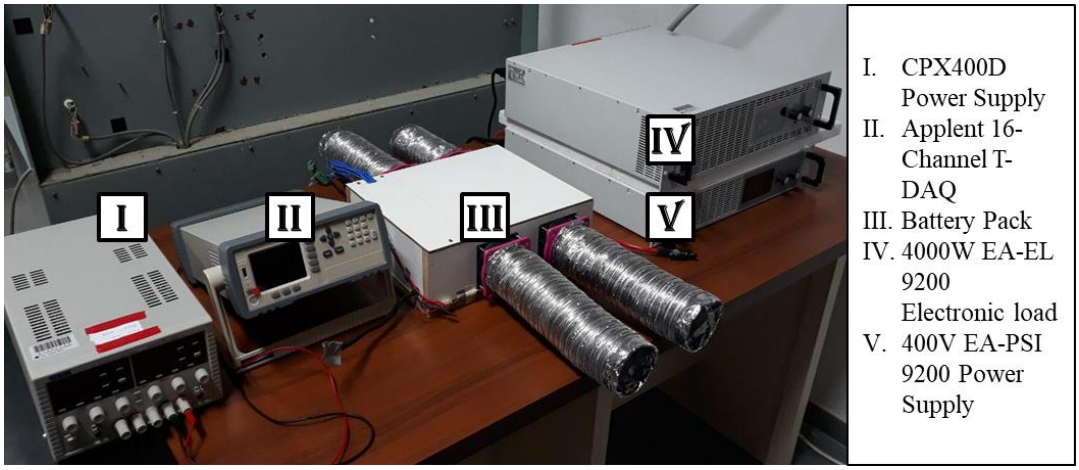

Figure 20: Experimental Setup

3.2.1 Battery Pack

The battery pack in the experimental setup is designed and built from Medium Fiberboard (MDF) of 18 cm thickness with four vent holes of 0.07m diameter drilled on the longest side face of the box (in Figure 21: I). The pack with dimensions (30*25*10) cm was built slightly larger than the exact volume of the battery module (24*24*10) cm. The extra volume in the MDF box was designed to create a partition that would accommodate excess length of thermocouple sensor wires attached to cells in the battery module (see Figure 21: II). This is to prevent unnecessary tension that would rather cause disconnection of sensor and cells in the battery module if the full length of the thermocouple wires were extended outside the box. Furthermore, glassfibre, (a nonconductive and nonflammable material) is placed between the battery module top cover of the MDF board as a protective measure to prevent possible electrical and fire hazards present during the experiment; and most importantly prevent a low resistance path for air flowing into the battery pack (Figure 21: III).

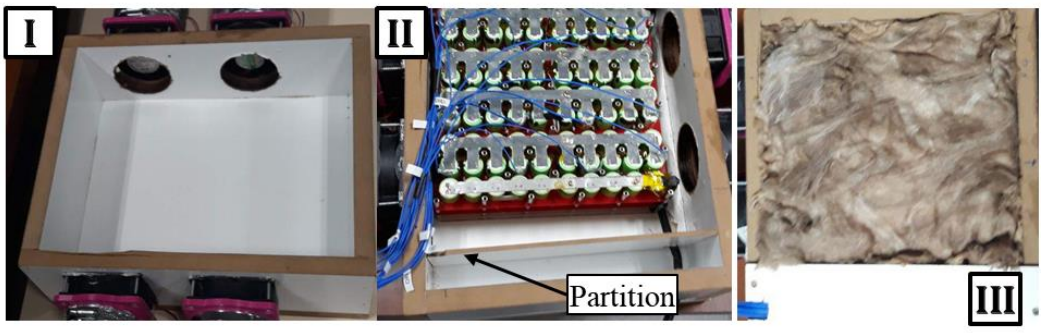

Figure 21: Battery Box Design

Table 5: Battery Pack Parameters

Volume Parameters (m^3)	
Total	0.0075
Partitioned	0.00125
Actual	0.00625
Vent Dimensions	
Diameter of Vent (m)	0.035
Area of vent (m^2)	0.003848
Two inlet vents (m^2)	0.007697
Volume Flow rate at various fan Speed (m^3/s)	
1.4	0.010776
2.4	0.018473
3.4	0.026169

3.2.2 Temperature Data Acquisitions Device

In order to monitor and record temperature of cells in the battery module during different charge/discharge rates, for various investigated design variables, we employed a 16-channel Applent Temperature Data Acquisition device shown in Figure 22.

Figure 22: Temperature Data Acquisition Device (T-DAQ)

The T-DAQ used in the experimental setup is powered by an ARM microprocessor that is capable of measuring temperatures from a variety of thermocouple types (T, J, K, E, etc.) at three sampling rates (fast, medium and slow), with a resolution of 0.1 °C. It allows for multiple units (°C, F, K) for recording temperature values

simultaneously from 16 channels onto a USB stick or directly onto a computer via a USB-Serial connection.

K-Type thermocouple sensors with lower and upper limits of 0 °C and 200 °C; has temperature ranges which are well within the limits of expected temperature rise of cells in the battery module to be tested, hence were employed during the experiment to measure and record temperature profile of cells.

Positions of Sixteen(16) Cells in the battery module was systematically selected for temperature measurements based on the assumptions that temperature of each selected cell will represent the local temperature of other cells in its surrounding. Meanwhile, a limiting factor; which is the number of channel the T-DAQ is limited to impacted the decision to monitor only 16 out of 100 cells in the battery module. The preexisting compact nature of the battery module also affected selection of cells to be monitored as well as the position of sensor attachments on each cell (see Figure 23).

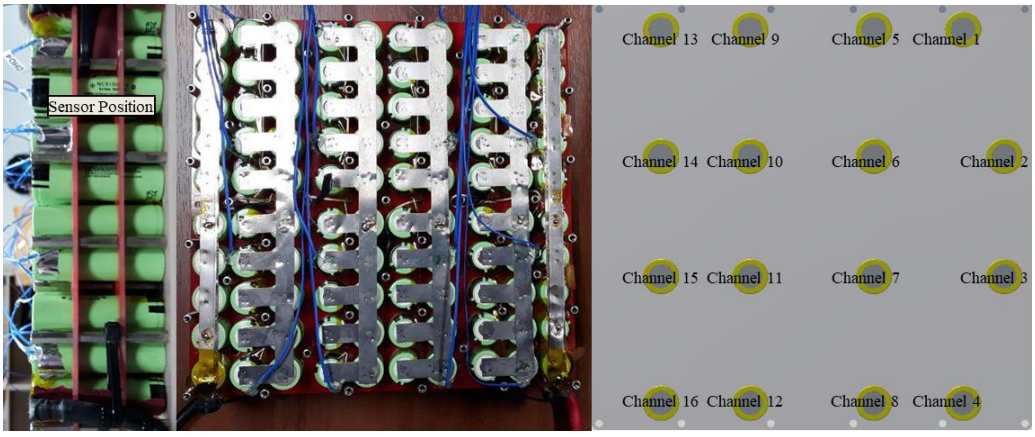

Figure 23: Thermocouple Position Selection and Attachment36

Despite the challenges faced during sensor attachment on selected cells, the following measures were taken to ensure proper contact between sensor and the cells:

- In order to ensure proper cell-sensor connection and improve conduction between the two entities, a thermal paste compound was applied around the sensor and the battery body, after which strips of a strong adhesive tape were used to secure the sensor to the body of the cell (see Figure 24).
- Silicone glue was applied to hold the protruding sensor wire at the attachment point on top of the cell terminal to provide for extra attachment strength (see Figure 24). Finally,
- Majority of the sensor wire length was kept folded in a separate partitioned section inside the MDF box to prevent accidental tension that might threaten or sever the connection between the sensor-cell attachment.

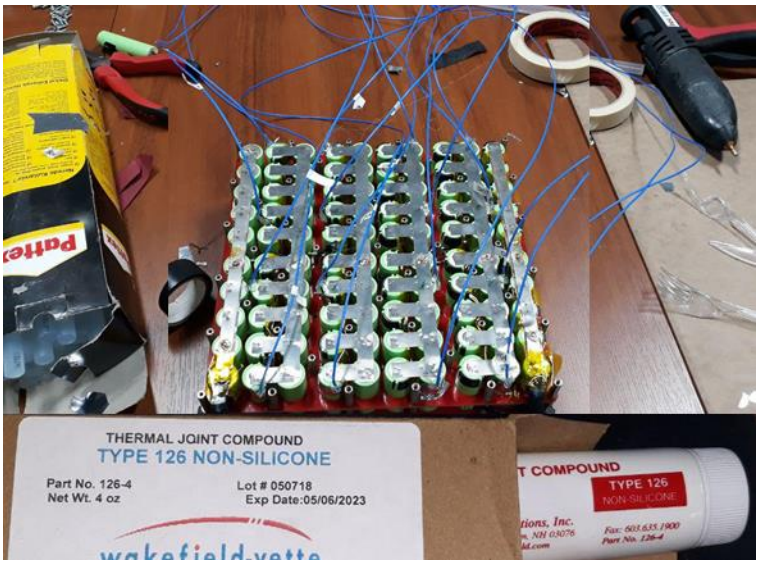

Figure 24: Sensor Attachment Measures

3.2.3 CPX400D Power Supply

To investigate the performance of the battery pack temperature wise, one design variable investigated was the rate at which cooling air was pumped into the battery pack. To achieve this, four (4) SMPS fans attached to the vents of the MDF box, were connected in parallel and routed via two connecting cables on the MDF box to be powered simultaneously, using the CPX400D power supply (see Figure 25). This method of connection ensured all the cooling fans operated at the same speed at any preset voltage.

Operating the SMPS fans in constant current mode, controlling the voltage input to the fans via the power supply allowed for the adjustment of power delivered to the fans hence controlling air flow speed into the battery pack.

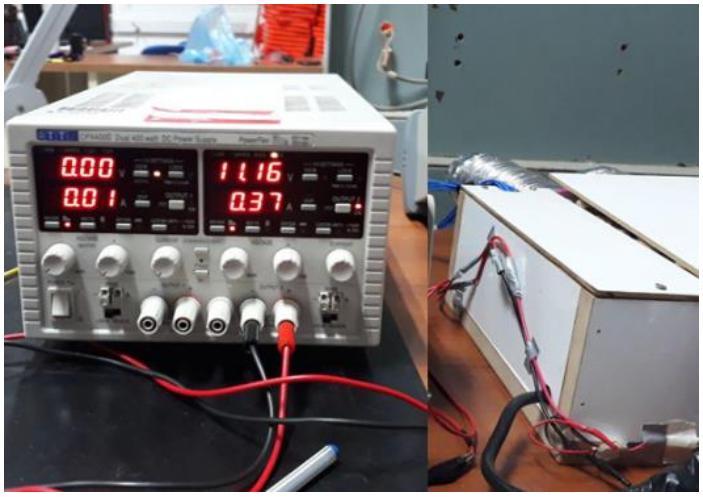

Figure 25: Controlling Fan Speed with CPX400D Power Supply

To investigate the battery pack in its base air flow configuration method, two adjacent fans were set for their airflow direction into the battery pack, while the other opposite fans were set to extract warm air out of the battery pack for active exhaustion.

This airflow configuration method was investigated for three airflow speed under two charge/discharge rates. Figure 26 shows the base air flow configuration of the battery pack investigated in this thesis.

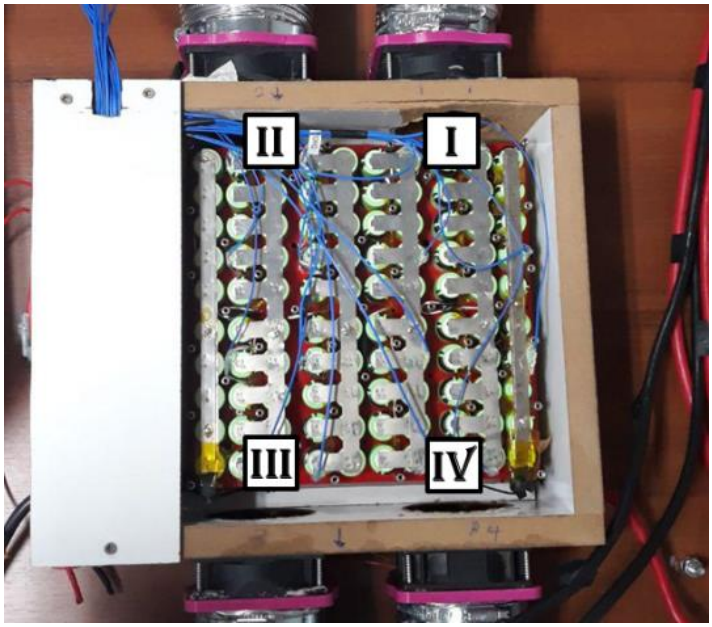

Figure 26: Battery Vent Configuration; Inlet Fans I & II, Outlet Fans: III & IV

3.2.4 Electronic Power Supply/Load

The electronic load and power supply used in this study were the "*Electro-Automatik"* heavy duty laboratory DC load and power supply. The version used in conducting the experiments; EA-EL 9200 electronic load is capable of an output of 4000W and the EA-PSI 9200 both operate at efficiencies of up to 95.5% (See Figure 27).

To test the battery pack module for charge and discharge cycles during the experiments, 50 Amps rated cables were used in connection between the battery pack the electronic load and power supply. Negative terminal cables of the electronic load, power supply and the battery module were permanently connected and their joints sealed, while the positive terminal for the systems were

connected/disconnected according to each experiment performed as part of safety measures observed.

Figure 27: EA Electronic Power Supply and Load

As tests on two current ratings on the battery pack module; 0.5 C and 0.75 C were to be investigated, the electronic load and power supply were programmed to a constant current rating of 0.5C, and the charge and discharge voltages are set to fit the specification of the battery module's upper and lower cut off voltages (see Table 6). The Graphical User Interface (GUI) of the load/supply provided real time voltage and current reading of the battery pack for monitoring purposes during charge/discharge cycles.

Table 6: Battery Module Specification

Ten (10) cells in series	Maximum Cutoff Voltage: (V): 4.2*10 = 42Volts	Minimum Cutoff Voltage(V): 3.2*10 = 32 volts
Ten (10) Cells in Parallel	Nominal Battery Module Capacity (Amp): 3.2*10 = 32 Amps	
Tested Capacity	0.75C	24 Amps
	0.5C	16 Amps

Chapter 4

EXPERIMENTAL PROCEDURE / METHODOLOGY

4.1 Designing of Experiments

This Study aims to investigate the thermal performance of a hundred (100) NCR18650 lithium cells battery module in a battery pack with four vents. The test process used in this study aims to simulate closely as possible near real time application scenario, hence ambient condition such as room temperature is considered an uncontrollable parameter so that little or no action is taken to control or alter ambient conditions during the test period.

After defining factors and their levels to be tested for experiment in this study, various DoE methods such as Plackett-Burman, Taguchi, Latin Square and Full Factorial, posed as viable methods to be used in planning and designing experiments to be carried out. After assessing various strength and features of each method, the *Full Factorial experiment design* was settled for, as it allowed for a study of main and interacting factors (air and current flow rate) effects on the battery module and also allowed for the development for a response surface of the design space tested. The full factorial method employed also provided the maximum number of experiments to be performed for the selected factors and levels. A total number of thirty-six (36) experiments were carried out (due to repetition) and twelve (12) unique experiments were analyzed after results of experiments with similar combinations of factors were averaged.

Table 7 below shows various factors and levels tested during the experiments and the experiments design development code using MATLAB.

Table 7: Design of Experiment Process

Factors	Levels
Current Rate (C)	0.5
	0.75
Airflow Rate (m/s)	1.4
	2.4
	3.4

```
% full factorial([2 levels of current rate, 3 levels of flow rate ])
>> DoE = fullfact([2,3])
DoE =
   1   1
   2   1
   1   2
   2   2
   1   3
   2   3
```

Experiment Map						
Repetition	0.5 C			0.75C		
	1.4 m/s	2.4 m/s	3.4 m/s	1.4 m/s	2.4 m/s	3.4 m/s
1	Charge	Charge	Charge	Charge	Charge	Charge
	Discharge	Discharge	Discharge	Discharge	Discharge	Discharge
2	Charge	Charge	Charge	Charge	Charge	Charge
	Discharge	Discharge	Discharge	Discharge	Discharge	Discharge
3	Charge	Charge	Charge	Charge	Charge	Charge
	Discharge	Discharge	Discharge	Discharge	Discharge	Discharge

4.2 Experiment Procedure

The Charge/ Discharge method employed while testing the battery pack performance followed the Constant Current – Constant Voltage (CC-CV) or Galvanostatic method. Employing this method of Charging, the battery module is initially charged at a specified current rate of 0.5C (16 Amps) from its minimum cutoff voltage of 32V till it barely reaches it maximum cutoff voltage typically 41.99V. At this state in the charging process, voltage is held at constant till the current flow rate reaches 0.3 – 0.2 Amps. At this point, the power supply or electronic load usually reaches their

minimum power limit typically at 0.2Amp (See Figure 28) hence the charging/discharging process is deemed completed.

Figure 28: Minimum Charge/Discharge Current Flow Rate

Before each cycle of experiment is begun, the cooling fans are inspected and set to the required level of air flow rate and measured with an anemometer. As the battery pack design employs two inlet cooling fans, the area of the vents calculated in Table 5 is doubled to determine the total volume of air being pushed into the battery pack at every set cooling fan speed.

After each charge/discharge cycle is completed, time is allowed for the cells in the battery module to rest in order to ensure electrochemical stability [11] before a new cycle commences. This waiting period also allow for the entire battery module reach a uniform temperature (usually the ambient temperature).

For each combination of levels of the investigated factors, the experiment is done three (3) times to ensure repeatability after which results are averaged. Repeating the experiment for each scenario of level combination, also allowed for battery testing to

be carried out for different ambient conditions. The temperature range of ambient temperature recorded during the entire period of the study ranged from 16°C during late nights and early mornings, to 24°C during mid-afternoons and evenings. Figure 29 illustrates systematic steps carried out performing each experiment cycle.

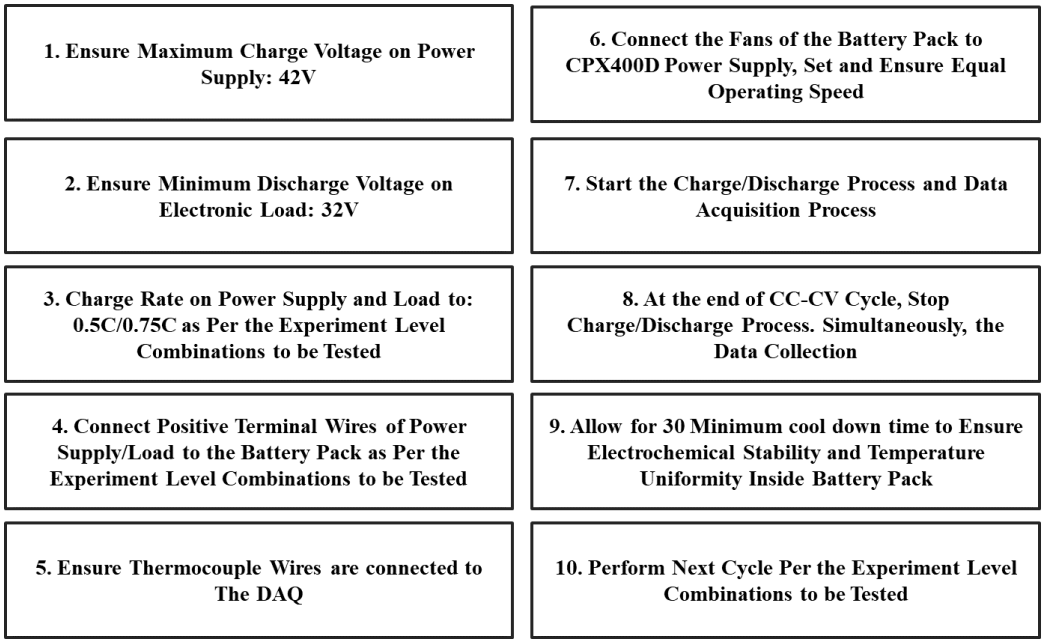

Figure 29: Experiment Cycle Procedures

4.3 Objective Functions Investigated

Temperature profiles of sixteen (16) cells from the battery module are monitored, and recorded by the K-type thermocouples and the T DAQ as the output variables of the experiment performed in this study. The sampling rate of the T DAQ was set to medium rate and a time of sixty seconds (1 min) is set as the interval between each temperature recording of the cells. An average of 172 temperature data point was generally recorded during the 0.5C current rate experiment and 150 data points during charging experiment with 0.75C current rate. Generally, lower times of discharging period were observed for 0.5C and 0.75C experiments.

The temperature values recorded during each charge/discharge cycle of experiment are automatically stored in a generic created file by the T-DAQ which is retrieved for data processing on a USB drive for data analysis.

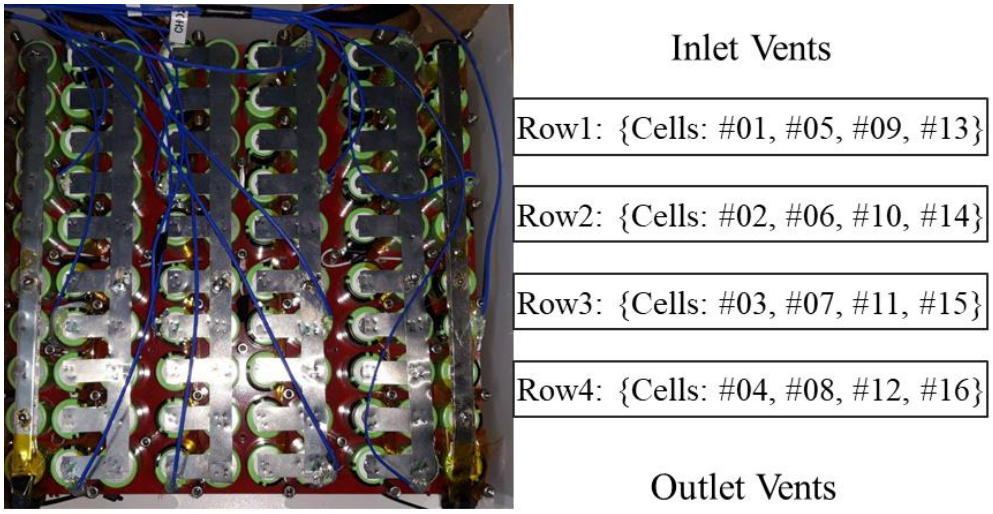

Figure 30: Sensor Position Nomenclature

For results analysis purpose the measured temperature values of selected cells in the battery module and the nomenclature depicted in Figure 30, will be adopted to address various individual cells, or a group of cells in a row.

4.3.1 Maximum Temperature (T_{MAX})

The performance and longevity of a cell operating under any given charge or discharge cycle greatly relies on its operating temperature not exceeding 40 °C [21], [22], [75] from literature survey and data specification of NCR18650 document. The maximum temperature (T_{MAX}) of any individual cell in a battery pack cooled under any battery thermal management system is therefore indicative of the overall performance of the BTMS.

For all the twelve experiments conducted in this study, combining each level of all the factors considered, the maximum temperature measured by any of the cells #01-

#16 over an entire charge/discharge cycle, is taken as the overall highest temperature in the battery pack for that specific air flow rate and current rate level combination.

4.3.2 Temperature Increase (T_{INC})

The Temperature increase (T_{INC}) represents the temperature difference between the Initial Temperature (T_I) and the Highest Temperature (T_H) of each measured cell in the battery pack. This measure, similarly to the maximum temperature of a cell in the battery pack is indicative of the performance of a BTMS but takes into consideration temperature profile of each measured cell. It also allows for the measure of temperature uniformity between cells in similar Rows one (1) through four (4) or sub modules. For a better BTMS performance, temperature uniformity between cells improves charging or discharge uniformity.

4.3.3 Temperature Difference (ΔT_{MAX})

The maximum allowable temperature between cells in a BP of 5°C has been reported in several studies including [21], [26], [27] and [28] , to promote battery balancing and uniform charging and discharging during the LiBs operating cycle. The average temperature of cells in each row will be determined and their differences presented as temperature difference in the battery module for each experiment performed.

Typically, an experiment with a combination of design levels which yields a temperature difference among various cell in a battery pack above 5 °C, would have performed poorly.

Chapter 5

RESULTS AND DISCUSSIONS

5.1 Thermal Performance of BTMS

The maximum temperatures experienced by monitored cells in the battery pack during the experiment performed in this study are obtained by averaging temperature values of experiments performed under similar combination of design variables after repetition. Figure 31 presents a capture of results of the entire test performed in this study plotting the maximum temperature for monitored cells in the battery pack for the two levels of current flow rate tested under all levels of air flow rate.

The data points are plotted based on their arrangements in the battery pack in respect to the cooling air flow path, so that maximum temperature (T_{MAX}) of cells in Row 1 {Cells: #01, #05, #9, #13} which are closest to the inlet vents are plotted first, following the systematic pattern through to cells in Row 4 based on the illustration presented in Figure 30.

From the graphs of results presented in Figure 31, a common trend in the thermal behavior of cells in Row1 irrespective of the current rate, operating cycle and the cooling air speed is that, they recorded the least maximum temperature. This can be associated to the fact that they naturally experience the effects of cooling air pumped into the battery pack at its ambient state in terms of temperature and speed. Another factor that plays greatly to this trend observed is that there is no presence of

accumulated heat generated by collective cells in the battery pack at the inlet vent area.

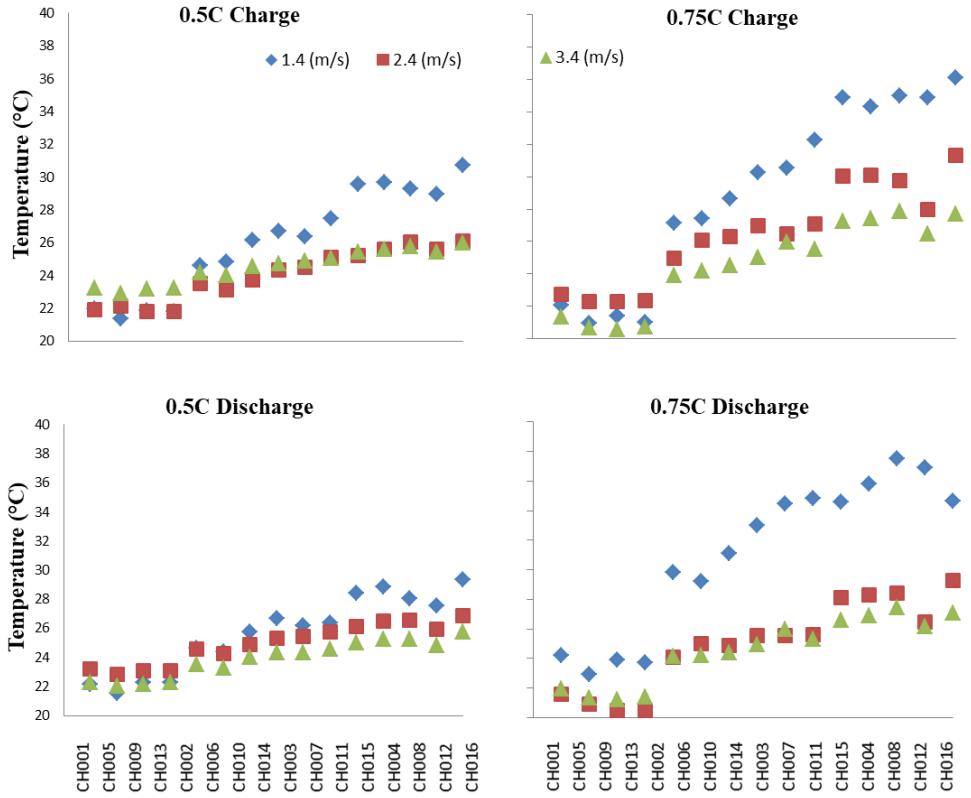

Figure 31: Thermal Characteristic of the Battery Pack

Another common trend observed in the results across all the graphs in Figure 31 is the relatively similar maximum temperatures in the battery packs during discharge cycle and the charge cycle experiment. Quantitatively, the absolute peak temperature obtained by the cell in channel 12 during the 0.5 C charge cycle is 30.7 °C and 29.3 °C during the discharge cycle under 1.4 m/s cooling rate.

Table 8 presents further comparisons for charge and discharge cycle for cell #06 observed during tests carried out in this study.

Table 8: Disparities in Maximum Temperature of Cells during Charge/Discharge Cycle

	0.5C		0.75C	
	Charge	Discharge	Charge	Discharge
1.4 m/s	30.70 °C	29.30 °C	36.10 °C	34.60 °C
2.4 m/s	26.07 °C	26.80 °C	31.10 °C	29.30 °C
3.4 m/s	26.00 °C	25.72 °C	27.70 °C	27.10 °C

In the data presented in Figure 31, there is a relative larger difference in the thermal behavior of the battery pack during its operation under cooling air flow rate of 1.4 m/s, as compared to the performance between air flow rates of 2.4 m/s and 3.4 m/s. The closeness in performance of the battery pack for airflow rate 2.4 m/s and 3.4 m/s is observed for charging and discharging under 0.5 C and for discharging under 0.75 C while the trend does not hold true for charging under 0.75 C. This break in trend, can be associated to the tendency of lithium ion cells to significantly generate heat at higher current rate and other factors such as heat accumulation in the battery pack.

The general increase in the trend of the maximum temperature registered for cells, as they move further away from the inlet vents observed for cells 1 through 16 in the entire test performed, can be associated to the effects of heat accumulation and increase in resistance of flow of the cooling air path. Similar effects have been reported in [27], [60] and measures such as bi-directional air flow have been proposed and investigated for battery packs to minimize cell maximum temperature and inter cells temperature difference, hence improving temperature uniformity in cells of a battery pack [27], [57], [60].

Upon critical study of the thermal result of the battery module presented in Figure 31, cell monitored by channel 12 of the T-DAQ is noticed to always record slightly lower temperatures than cells in its locality (Row 4). Upon investigating this

behavior, it was observed that Cell 12 happens to be directly in front of an exhaust vent hence it is hypothesized that cell 12 experienced slightly better cooling as heated air in the battery pack was constantly vented from its position. This phenomenon would also prevent heat accumulation at that locality.

Finally, comparing results obtained for the battery pack performance presented in this study to set allowable BP maximum temperature, an averaged maximum temperature of was 36.1 °C was obtained for 0.75 C charge experiments at 1.4 m/s flow rate and a temperature value of 37.5 °C for after three repetition of discharging at 0.75 C and 1.4 m/s. In a real life application, charging under such condition (0.75 C & 1.4 m/s) would not be recommended as the optimal temperature for operating lithium ion cells is 40 °C [75], [76]; a value which the worst obtained results in this study is 4 to 5 °C shy of.

Conclusively, in scenarios where power consumption of a BTMS system is of an objective function to minimize, cooling at speeds higher than 2.4 m/s would not be recommended for current rate less than 0.75 C during charge or discharge cycle, as the results in Figure 31 shows no significant (difference in T_{MAX}) improvements in BTMS performance when changing air flow rates from 2.4 m/s to 3.4 m/s.

5.2 General Effects of Air Flow Rate

From research conducted in the literature review stage of this study, the general trend observed in many published research in the field of air cooled BTMS is that; higher cooling air flow rate yields better BTMS performance in terms of the objective functions; *minimization of maximum cell temperature, increase temperature uniformity amongst cells and minimize temperature differences between cells*.

5.2.1 Effects of Air Flow Rate on T_{MAX}

Upon analysis of the test results conducted in this study, a similar trend has been observed for the battery pack model presented and tested in this study. Figure 32 shows a general downtrend in maximum Temperature recorded as air flow rate is increased. The test results presented in Figure 32 just as in Figure 31 are obtained after averaging temperature data recorded for unique experiments after repetition.

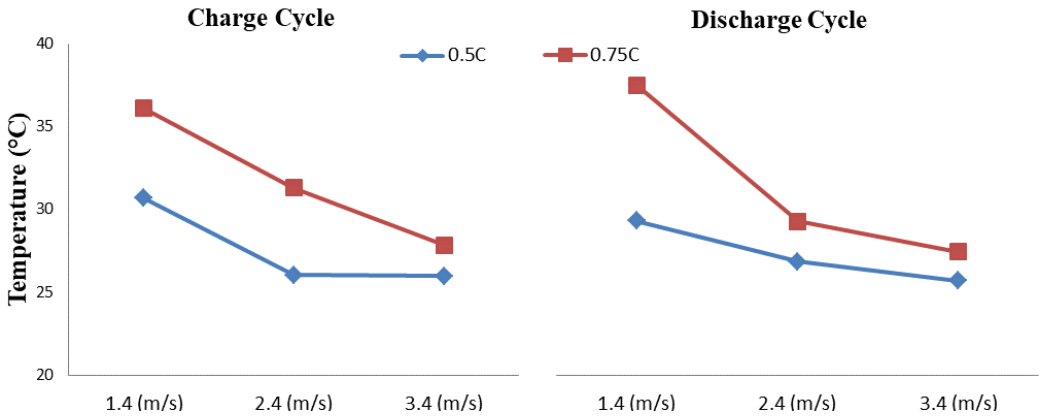

Figure 32: Effects of Increasing Air Flow Rate on Maximum Temperature

5.2.2 Effects of Air Flow Rate on ΔT_{MAX}

Analyzing the performance of the battery pack for temperature difference among cells under various experiment combinations of design variables, the average temperature of cells in each Rows one through four, is further calculated for all the individual unique experiment for this analysis. This measure taken reduces the measured temperature output from sixteen cells to four cells classified by their positions in the battery pack (see Figure 30). After classification of all sixteen cells into four rows, the maximum temperature in each row is determined. Lastly, the absolute difference in T_{MAX} between all the combinations of Rows is presented in Figure 33 and Figure 34.

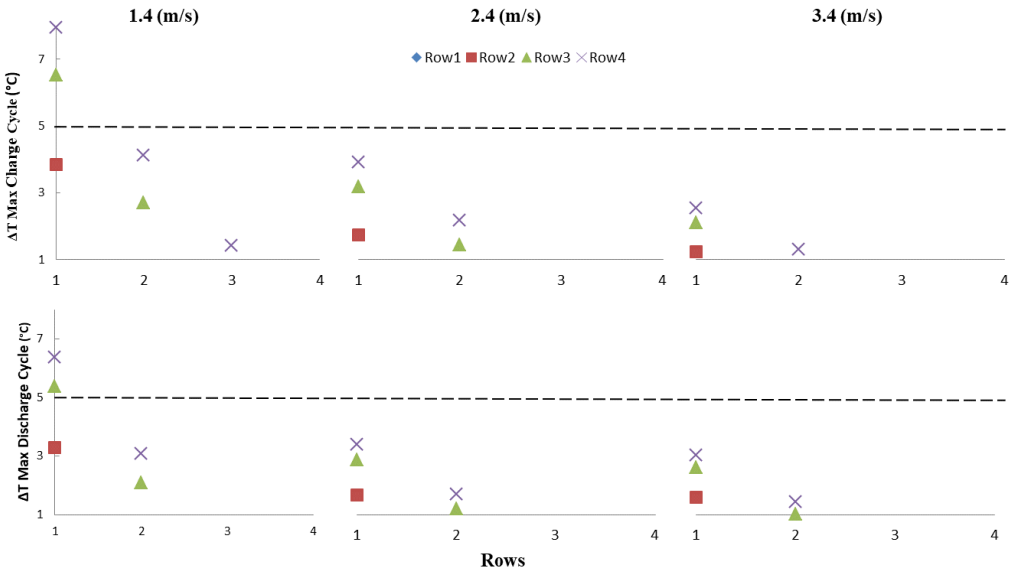

Figure 33: Effects of Air Flow Rate on Temperature Differences (0.5C)

In Figure 33, it is observed that for the lower current rate of 0.5 C tested; the majority of temperature difference between rows of cells measured in the battery pack is below 5 °C which is the recommended maximum temperature difference between cells in a battery pack cooled by any BTMS.

The maximum temperature difference measured during experiments conducted under the 0.5 C current rate is recorded to be 8°C during a charge cycle under 1.4 m/s and 6.37 °C for a discharge cycle under the same flow rate which occurred between cells in Row1 and Row4.

For flow rates of 2.4 and 3.4m/s tests under 0.5C, the temperature difference between all interacting Rows in the BP was kept well below 5°C.

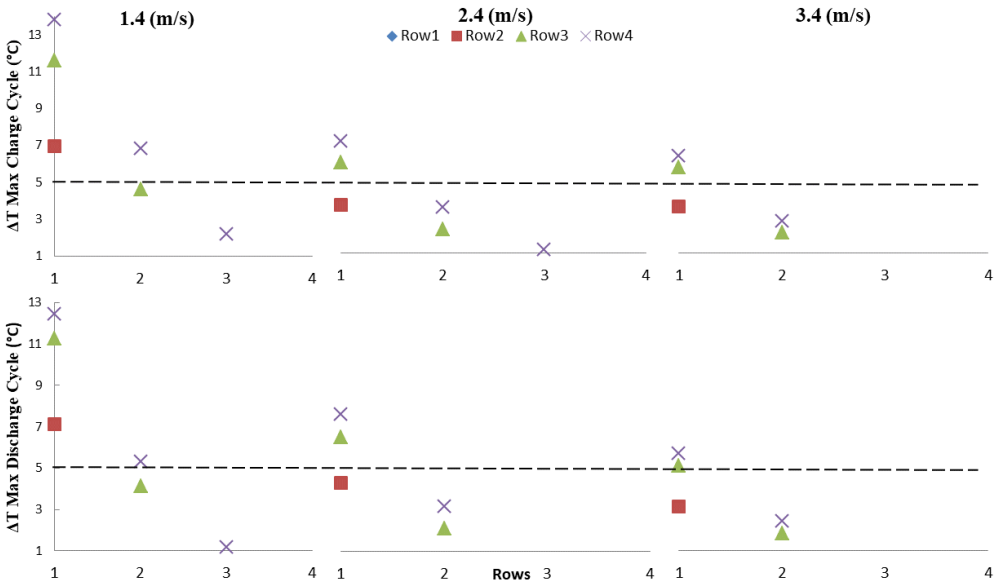

Figure 34: Effects of Air Flow Rate on Temperature Differences (0.75 C)

Figure 34 which plots the cell temperature difference for experiments conducted under 0.75 C current rate, the temperature difference between cells in (Row 1 and Row 2), (Row 1 and Row 3), (Row 1 and Row 4) and (Row 2 and Row 4) were observed to be above the 5 °C threshold of under air flow rate of 1.4m/s during charge and discharge experiments. As the air flow rate increases to 2.4m/s, the temperature difference which occurred under the charge cycle is reduced from three to two interactions (Rows1 and Rows 3, Rows 1 and Rows4) similar to results obtained for 0.5 C charge experiment under 1.4 m/s.

Temperature differences between Rows 1 and 4 during the charge and discharge cycle recorded under 0.75 C were as high as 13.81 °C and 12.42 °C respectively for the least flow rate and reduced to 6.0 °C and 5.25 °C under air flow rate of 3.4 m/s.

Assessing the battery pack based on the performance of results obtained from temperature difference between cells, air flow rate higher than 3.4 m/s for the battery module and battery pack design presented in this study is recommended, as results

show that the cooling method employed during the testing, yielded temperature difference between cells greater than 5 °C on every instant of testing for the higher current flow rate of 0.75 C.

5.3 Battery Pack Model Development

In this section, two model development techniques are applied on the data sets obtained from the experiments in this study. Raw input data described in Table 9 and maximum temperature values obtained from 16 monitored cells, are used as input and output training data for an ANN algorithm to develop a model for the battery pack investigated in this study.

All 12 unique current rate and air flow rate level combination experiments developed by the full factorial DoE method are used as input data [X, Y] with the averaged absolute maximum temperature of each unique experiment is used as an output [Z] to develop a surface regression model.

5.3.1 Artificial Neural Network

Artificial Neural Network (ANN) is a set of interconnected neurons that mimic the information processing similar to humans. It provides functions to create train, visualize and simulate neural networks capable of performing classification, regression, clustering, time-series forecasting and dynamic modeling [77], [78]. A neural network consist of a two layer feed- forward network with sigmoid hidden neuron and linear output neurons that can fit multidimensional mapping problems arbitrarily, when given consistent data and enough neurons in it.

Several types of neural network and how they are applied to solve specific problems they are suited for, have been demonstrated in literature. Peculiar to research in lithium ion batteries, X. Qian, et al. in [79] applied artificial neural network in

optimization of their design parameters, for a proposed battery pack model; and H. Sassi et al. applied ANN to a set of empirical data, to develop a model to predict the SOC level of lithium ion cell studied in their work [77].

In this study, an ANN architecture model (Figure 35) is trained offline with input data set from all experiments conducted. Input data such as Charge cycle (Represented as 1), discharge cycle (represented as 0), the ambient temperature during the experiment, the current rate, and the air flow rate (Table 9) while the maximum temperature of all monitored cells are fed as an output data to the neural network. In total, a matrix of 4 by 37 and 16 by 37 data size were used as input and output data sets respectively used in the training phase of the ANN model development.

Table 9: ANN Input Training Data Sample

Experiment	Cycle	Flow rate (m/s)	Current Rate (C)	Ambient Temp °C
0.5DS1T3	0	1.4	0.50	17.10
0.75DS2T1	0	2.4	0.75	18.76
0.75CS1T1	1	1.4	0.75	19.08

After several iteration of training, a model obtained with an R value of 0.99139 was obtained between the fitted model and the given training data, 0.98112 correlation R value between the fitted model and the given data for testing and an R value of 0.98869 for an overall correlation between the actual outputs and the targets as displayed in Figure 36.

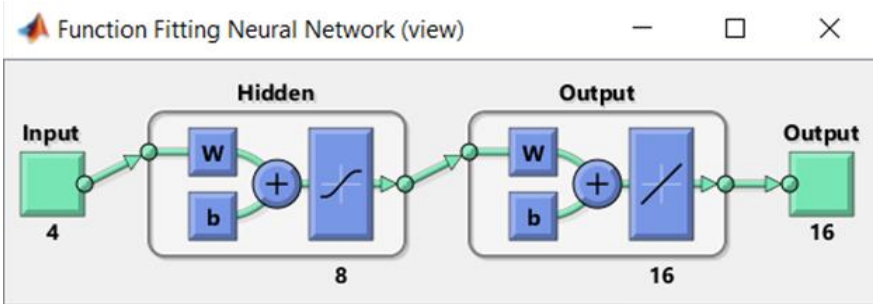

Figure 35: ANN Architecture

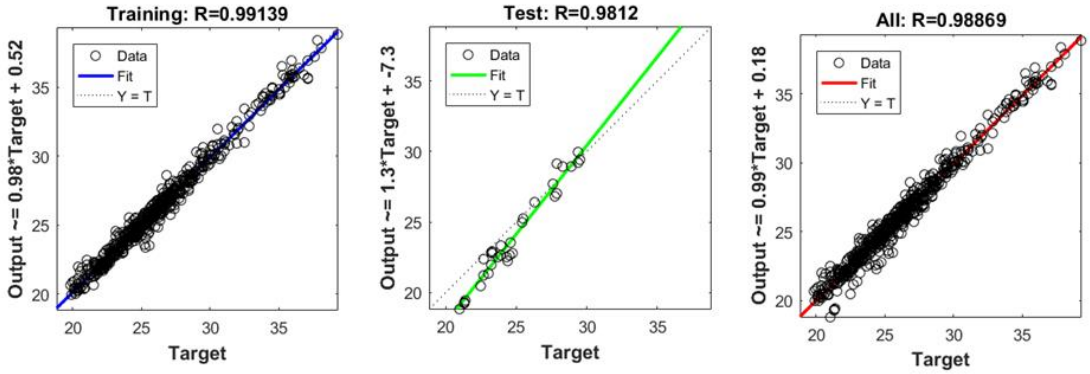

Figure 36: ANN Regression Plot

The training algorithm selected for training this ANN model in this thesis was the '*Bayesian Regularization'* algorithm for its performance with difficult small and noisy data set [78]; a critical feature of the data output obtained during the conducted experiments in this study.

5.3.2 ANN Model Validation/ Error Analysis

A Simulink (Figure 37) model and a MATLAB function code was generated after ANN training which is capable of predicting the behavior of the battery pack tested within the limits of the trained input data.

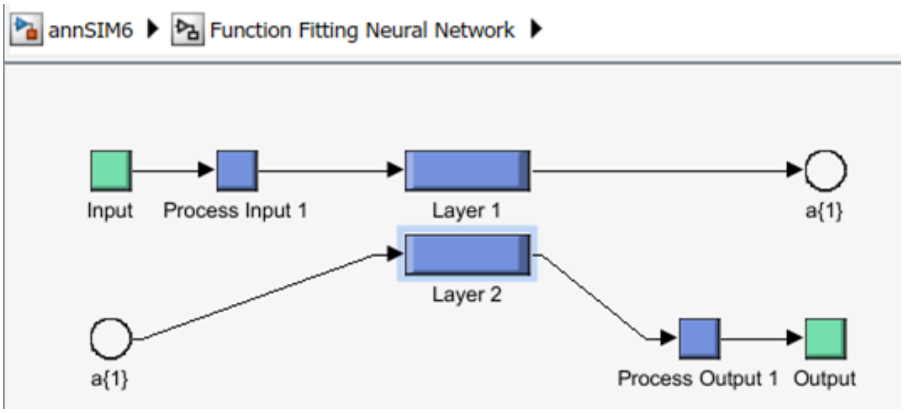

Figure 37: ANN Simulink Model

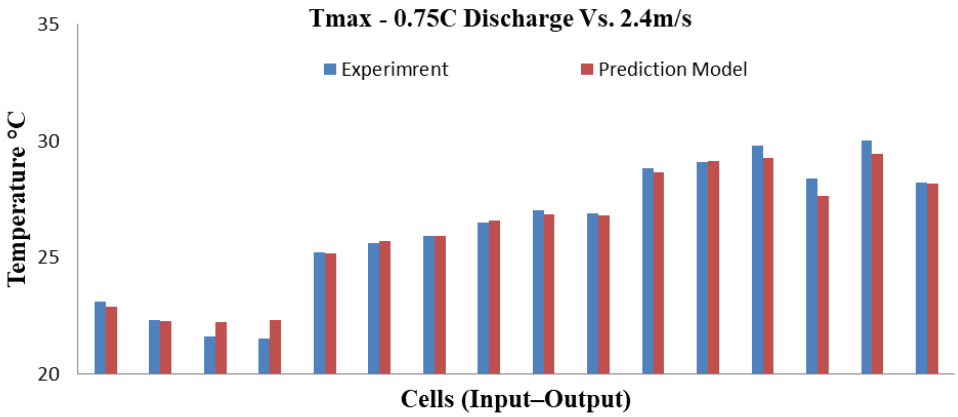

Figure 38: Predicted T_{max} versus Actual Value

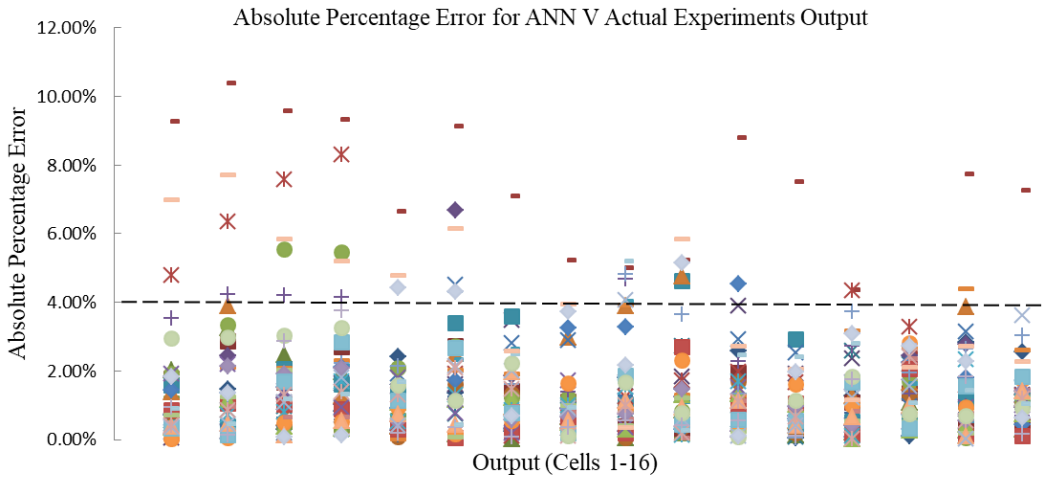

Figure 39: Percentage Error between Real Output and Predicted Output Values for Entire Experiments

Figure 38 shows the maximum temperature comparison between empirically obtained data for a discharge cycle experiment conducted under 0.75 C current rate and 2.4 m/s air flow rate versus the obtained Maximum temperature values predicted by the trained model for the same experiment. While the displayed result in Figure 38 shows a closely relation between the experiment and predicted model output with an absolute maximum percentage error of 1.84%, Figure 39 illustrate the error percentage graph between predicted and actual maximum temperature for the entire experiments. Figure 39 showed the ANN model prediction correlates with the actual output accurately, with 93% of the predictions below 4% absolute error. 6.5% of the predicted output by the ANN model fell above 4% absolute error and a maximum percentage between a predicted and an actual output of 10.38% error was calculated.

5.3.3 Response Surface Model (RSM) Development

RSM comprises of regression surface fitting over a bounded design space to predict approximated responses for input variable combinations not accounted for during a physical or simulation experiment [80]. Usually, a Design of Experiment method is used to obtain minimum number of experiments needed to develop an RSM. In the RSM method implemented in this study, the approximation function used in developing the response surface, is a second degree polynomial. Most response surfaces functions are generated with polynomials, depending on number of data points from an experiment provided.

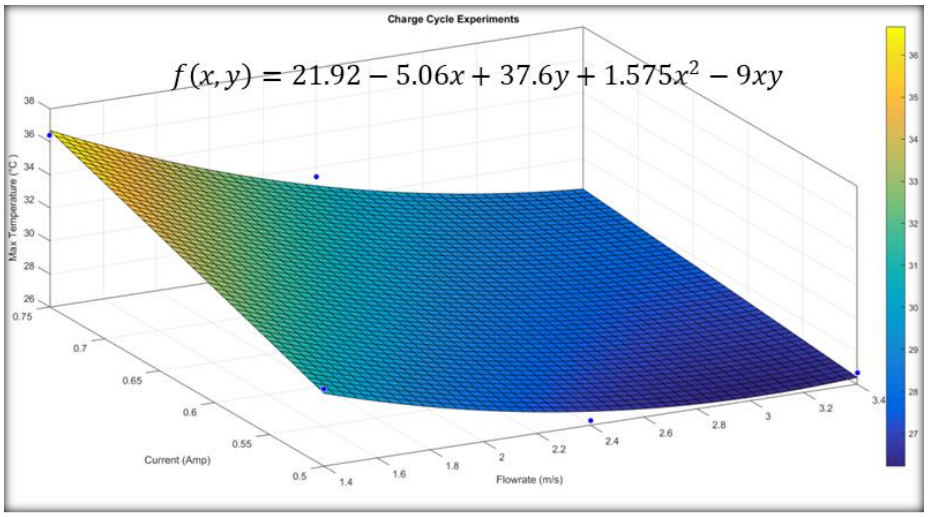

Goodness of Fit: SSE- 0.9075, R^2- 0.9875, Adjusted R^2- 0.9373

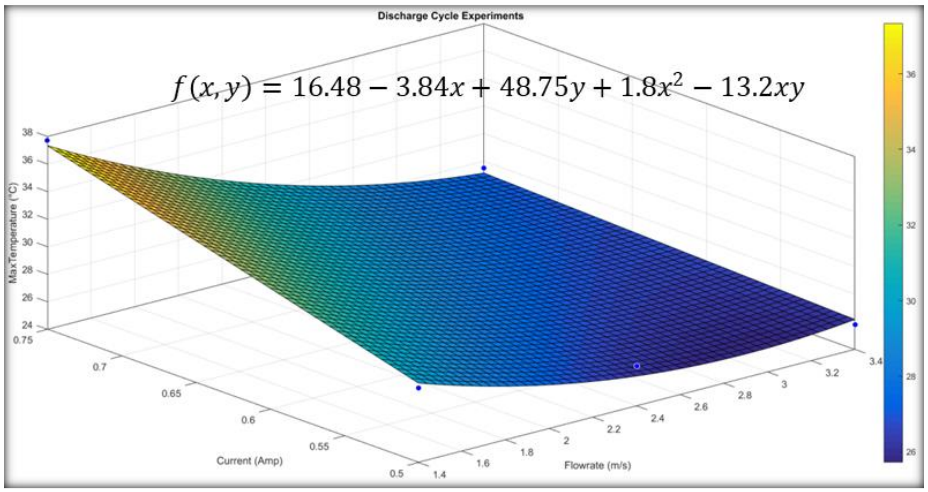

Goodness of Fit: SSE- 1.6133, R^2- 0.9824, Adjusted R^2- 0.9121

Figure 40: RSM Developed for Charge and Discharge Experiment

The RSM developed for the battery model was done using the MATLAB curve fitting tool box. Fitting parameters *R^2 adjusted* was used to determine the goodness of fit, *Sum of Square Error (SSE)* and *Mean Square Error (MSE)* were used to determine the predictability of the model.

R^2 adjusted values lies between 0 and 1 for which a good response surface has a value is closest to 1 [80], [81]. On the contrary, an SSE and MSE values which closer to zero are desired for a good response surface. An SSE value closer to zero indicates a model has smaller random error component, hence higher prediction

accuracy [81]. Just as SSE, an MSE value closest to zero is desired for a good response model.

After many variations of the fit method applied on the variables were tested to obtain the best adjusted R^2 and SSE values, the model was developed with the polynomial function having robustness "*off*" as this trial produced the most suitable fitness parameters results (see Table 10).

Table 10: Comparison of Various Fitness Parameters for the Developed Regression Model

2^{nd} Degree Polynomial Fit					
Robustness:			Off		
	Fit Type	SSE	RMSE	R^2	Adjusted R^2
Charge	poly21	0.9075	0.9526	0.9875	0.9373
Discharge	poly21	1.6133	1.2702	0.9824	0.9121
Robustness:			LAR		
Charge	poly21	0.9075	0.9526	0.9875	0.9373
Discharge	poly21	1.6133	1.2702	0.9824	0.9121
Robustness:			Bi-Square		
Charge	poly21	1.3491	1.1615	0.9814	0.9068
Discharge	poly21	2.3984	1.5487	0.9739	0.8693

The model equations of the RSM developed for the charge and discharge experiments performed for the battery pack and module in this study is presented as:

$$\boldsymbol{f(x,y) = P_0 + P_1x + P_2y + P_3x^2 + P_4xy} \quad \textbf{(1)}$$

Where x and y are designed variables *air flow rate* and *current rate* respectively, $P_0 - P_4$ are coefficient constants and $f(x,y)$ is the design objective of minimization. Table 11 presents coefficient values for the developed model equations.

Table 11: Model Equation Coefficients

	Charge	Discharge
P_0	21.92	16.48
P_1	-5.06	-3.84
P_2	37.6	48.75
P_3	1.575	1.8
P_4	-9	-13.2
Goodness of Fit		
Charge:	SSE- 0.9075, R^2- 0.9875, Adjusted R^2- 0.9373	
Discharge:	SSE- 1.6133, R^2- 0.9824, Adjusted R^2- 0.9121	

5.3.4 RSM Model Validation / Error Analysis

In an attempt to validate the regression model developed in this study, equations of the developed RSM's are tested for experimental inputs to compare the output results. Figure 41 plots and compares predicted absolute maximum temperatures against actual maximum temperatures for charge experiment at 0.5 C and discharge experiment for 0.75 C.

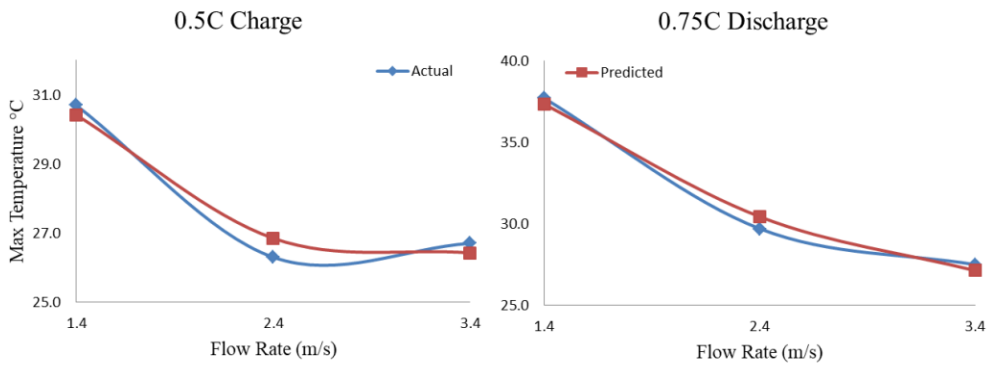

Figure 41: Regression Model Predicted Output VS Actual Output for a Sample Input

Table 12 below shows the absolute relative error calculations between the predicted model and the actual outputs for absolute maximum temperature in a battery pack for all the twelve unique experiments performed. The results showed the developed model predicts accurately with an absolute maximum error of approximately 3.00%.

Table 12: Absolute Relative Error between Regression Model and Actual Experiment

	Charge at 0.5 C			Discharge at 0.5 C		
	1.4 (m/s)	2.4 (m/s)	3.4 (m/s)	1.4 (m/s)	2.4 (m/s)	3.4 (m/s)
Actual (°C)	30.70	26.30	26.70	29.40	26.90	25.80
Predicted (°C)	30.42	26.85	26.42	29.77	26.17	26.17
% Error	**0.91%**	**2.08%**	**1.04%**	**1.25%**	**2.72%**	**1.42%**
	Charge at 0.75 C			Discharge at 0.75 C		
	1.4 (m/s)	2.4 (m/s)	3.4 (m/s)	1.4 (m/s)	2.4 (m/s)	3.4 (m/s)
Actual (°C)	36.40	31.40	27.90	37.70	29.70	27.50
Predicted (°C)	36.67	30.85	28.17	37.33	30.43	27.13
% Error	**0.75%**	**1.76%**	**0.98%**	**0.97%**	**2.47%**	**1.33%**

Chapter 6

CONCLUSION

In this study, a Battery Thermal Management System (BTMS) for a battery pack housing a battery module consisting of hundred NCR18650 Lithium ion cells has been designed and tested in relatively cold ambient conditions.

The battery pack designed, featured four vent holes of which two adjacent ones operated as inlet vents for cooling air and the other two as exhaust vents. It also featured a partitioned volume that housed portions of sensor cables used for monitoring cell temperature during charging and discharging experiments.

The BTMS performance is tested for two major objective function criterions which are:

- Maximum Temperature recorded by a cell in the battery pack at any instant should be kept below 40 °C and
- Maximum Temperature difference between any cells in the battery pack during testing should not exceed a threshold of 5 °C.

The maximum temperature and maximum temperature difference limit threshold is obtained from various literature reviews and battery data specification documents.

Design variables - three levels of cooling air flow rate and two levels of current rate are combined in a full factorial design of experiment method to develop a full array of experiments that was performed on the BTMS for the battery pack. Each

experiment performed consisted of a charge and discharge cycle repeated three times to achieve repeatability in experimentation.

After experimentation it was observed in results that discharge cycles under any experiment variable combination rarely produces similar maximum temperature than their charge cycle. Another common observation made was that higher current rate experiments produced relatively higher maximum temperature amongst the cells. However, significant change in maximum cell temperature and temperature difference are observed as airflow rate is increased. Lower air flow rate tended to produce higher maximum temperature and temperature difference among cells, hence producing an undesirable BTMS performance.

A 15.09% reduction in maximum temperature recorded by a cell was achieved during a charging experiment with 0.5 C current rate by increasing the air flow rate from 1.4 m/s to 2.4 m/s. For the same charge experiment, there was no significant improvement in the maximum temperature recorded at a higher air flow rate of 3.4 m/s. On the contrary, at higher current rate of 0.75 C charging, a 13.20% reduction in maximum temperature of a cell was achieved by increasing the airflow rate from 1.4 m/s to 2.4 m/s, and further increment of the air flow rate to 3.4 m/s produced a 22.81% reduction in the maximum cell temperature.

The results obtained points to a hypothesis that for the investigated battery pack design, for each current rate, there exist an optimal cooling airflow rate that if exceeded, will yield little or no improvement in an operating BTMS performance at a specific range of ambient condition. This hypothesis will prove vital in scenarios where power consumption of an operating BTMS is a critical objective function to

be minimized. Also in the development of an intelligent/dynamic BTMS where cooling operation of a BTMS will operates in a dynamic mode depending on the current profile the battery module.

Assessing the BTMS performance based on temperature difference among cells, it was observed that cooling air flow rate of 1.4 m/s for every charge/discharge cycle experiment, there was always an instant where the maximum temperature difference between any of the monitored cells exceeded 5 °C reducing the performance of the BTMS under this condition. However at higher speeds of 2.4 m/s and 3.4 m/s, charging and discharging under 0.5C, the temperature difference among cells in the battery pack was found to be always below the 5 °C threshold.

Charging and Discharging at 0.75 C under 1.4 m/s, 100% of the interactions between cells in Rows 2, 3 and 4 with Row 1 was observed to exceed 5 °C with the maximum recorded difference measured at 13.81 °C and occurred between cells in Row 4 and Row 1. However, increasing the airflow rate during the charge and discharge cycle under 0.75 C, the interaction of Rows 2, 3 and 4 with Row 1 which exceeded 5°C reduced by 33.33%. The highest temperature recorded under 0.75 C with 2.4 m/s was found to be 7.71 °C (a 44.14% reduction form operation under 1.4 m/s) and 6.3°C (a 54.38% reduction form operation under 1.4 m/s) for 3.4 m/s between cells in Row 4 and Row 1.

These observations aid in affirming the conclusion based on literature that; higher cooling air flow rates reduces maximum cell temperature and temperature difference between cells in a battery pack due to the increased convective heat transfer coefficient of air at higher velocities. However, the gradient in temperature

difference amongst cells remains the same with at least a single case of interaction between cells at different position in the battery module exceeding 5℃ for the investigated battery module. To fully obtain an air cooled BTMS performance where in the possibility of no interacting cells in the battery module has ΔT_{max} exceeding 5℃, a bidirectional cooling flow path scheme must be implemented.

6.1 Future Works

In this section, proposed solutions to challenges that affected some decision and design variable selection during the experimentation phase of this study are highlighted:

i. The preexisting nature of the battery module tested, made it almost impossible to monitor selected cell temperatures at more than one location. Future easy accessibility to the entirety of the cells body in the battery module will make it possible for each temperature profile of 16 cells to be monitored at more than one location. This will further improve the reliability of the data collected also make for more training data for ANN model development.

ii. The performance limits of the SMPS fans implemented during experimentation played a major role in selecting the maximum and minimum limit for cooling air flow rate. Implementing cooling fans with higher power rating in a future study will allow for the level of air flow rate factor be increased; enabling testing effects of higher cooling air flow rates and higher current rates.

iii. Implementing cooling fans with inbuilt temperature sensors in future works will allow for dynamic operation of the fans at certain battery pack temperature limits improving the nature of the study.

iv. Also, data of the sensitive ambient temperature changes as a measured output parameter in a future study would allow for an in-depth study of a battery module thermal performance in relation to changing ambient conditions for a set of given cooling and current flow rate. This understanding will also improve the performance of a dynamic BTMS such that cooling air flow rate is adjusted in real time for a battery pack or cooling air is preconditioned optimally based on a changing ambient condition.

v. Finally, in future works, the development of a full simulation model for the investigated experimental setup in this study will allow for multiple variation of design variables and parameters be controlled and their effect on a BTMS be monitored for optimization purposes.

REFERENCES

[1] J. Kim, J. Oh, and H. Lee, “Review on Battery Thermal Management System for Electric Vehicles,” *Appl. Therm. Eng.*, vol. 149, no. September 2018, pp. 192–212, 2018.

[2] IEA, “Global EV Outlook 2017 Together Secure Sustainable Global EV outlook 2017,” *Int. Energy Agency*, 2017.

[3] W. Wu, S. Wang, W. Wu, K. Chen, S. Hong, and Y. Lai, “A critical review of battery thermal performance and liquid based battery thermal management,” *Energy Convers. Manag.*, vol. 182, no. January, pp. 262–281, 2019.

[4] H. Budde-Meiwes *et al.*, “A review of current automotive battery technology and future prospects,” *Proc. Inst. Mech. Eng. Part D J. Automob. Eng.*, vol. 227, no. 5, pp. 761–776, 2013.

[5] L. Li, F. Dababneh, and J. Zhao, “Cost-effective supply chain for electric vehicle battery remanufacturing,” *Appl. Energy*, vol. 226, no. June, pp. 277–286, 2018.

[6] J. Adolf *et al.*, “Shell Hydrogen Study Energy of the Future? Sustainable Mobility through Fuel Cells and H2,” Jan. 2017.

[7] J. Shim, R. Kostecki, T. Richardson, X. Song, and K. . Striebel, “Electrochemical analysis for cycle performance and capacity fading of a

lithium-ion battery cycled at elevated temperature," *J. Power Sources*, vol. 112, no. 1, pp. 222–230, Oct. 2002.

[8] S. S. Zhang, K. Xu, and T. R. Jow, "The low temperature performance of Li-ion batteries," *J. Power Sources*, vol. 115, no. 1, pp. 137–140, Mar. 2003.

[9] S. Arora, "Selection of thermal management system for modular battery packs of electric vehicles: A review of existing and emerging technologies," *J. Power Sources*, vol. 400, no. September, pp. 621–640, 2018.

[10] L. Ianniciello, P. H. Biwolé, and P. Achard, "Electric vehicles batteries thermal management systems employing phase change materials," *J. Power Sources*, vol. 378, no. January, pp. 383–403, 2018.

[11] E. GÜMÜŞSU and Ö. EKİCİ, "THERMAL MODELING OF LITHIUM ION BATTERIES LİTYUM İYON PİLLERİN ISI L MODELLEMESİ," Hacettepe University, 2017.

[12] N. Yang, X. Zhang, G. Li, and D. Hua, "Assessment of the forced air-cooling performance for cylindrical lithium-ion battery packs: A comparative analysis between aligned and staggered cell arrangements," *Appl. Therm. Eng.*, vol. 80, pp. 55–65, 2015.

[13] V. Etacheri, R. Marom, R. Elazari, G. Salitra, and D. Aurbach, "Challenges in the development of advanced Li-ion batteries: a review," *Energy Environ. Sci.*, vol. 4, no. 9, p. 3243, Aug. 2011.

[14] “Basic to Advanced Battery Information from Battery University.” [Online]. Available: https://batteryuniversity.com/. [Accessed: 16-Jun-2019].

[15] J. Y. Yong, V. K. Ramachandaramurthy, K. M. Tan, and N. Mithulananthan, “A review on the state-of-the-art technologies of electric vehicle, its impacts and prospects,” *Renew. Sustain. Energy Rev.*, vol. 49, pp. 365–385, Sep. 2015.

[16] B. Lei, W. Zhao, C. Ziebert, N. Uhlmann, M. Rohde, and H. Seifert, “Experimental Analysis of Thermal Runaway in 18650 Cylindrical Li-Ion Cells Using an Accelerating Rate Calorimeter,” *Batteries*, vol. 3, no. 2, p. 14, 2017.

[17] C.-Y. Jhu, Y.-W. Wang, C.-Y. Wen, and C.-M. Shu, “Thermal runaway potential of LiCoO2 and Li(Ni1/3Co1/3Mn1/3)O2 batteries determined with adiabatic calorimetry methodology,” *Appl. Energy*, vol. 100, pp. 127–131, Dec. 2012.

[18] O. S. Mendoza-Hernandez, H. Ishikawa, Y. Nishikawa, Y. Maruyama, and M. Umeda, “Cathode material comparison of thermal runaway behavior of Li-ion cells at different state of charges including over charge,” *J. Power Sources*, vol. 280, pp. 499–504, Apr. 2015.

[19] D. P. Abraham, E. P. Roth, R. Kostecki, K. McCarthy, S. MacLaren, and D. H. Doughty, “Diagnostic examination of thermally abused high-power lithium-ion cells,” *J. Power Sources*, vol. 161, no. 1, pp. 648–657, Oct. 2006.

[20] C.-V. Hemery, “Etudes des ph ´ enes thermiques dans les batteries Charles-Victor Hémery Etude des phénomènes thermiques dans les batteries Li-ion,” 2014.

[21] K. Li, J. Yan, H. Chen, and Q. Wang, “Water cooling based strategy for lithium ion battery pack dynamic cycling for thermal management system,” *Appl. Therm. Eng.*, vol. 132, pp. 575–585, 2018.

[22] M. Al-Zareer, I. Dincer, and M. A. Rosen, “Performance assessment of a new hydrogen cooled prismatic battery pack arrangement for hydrogen hybrid electric vehicles,” *Energy Convers. Manag.*, vol. 173, no. April, pp. 303–319, 2018.

[23] Y. Deng *et al.*, “Effects of different coolants and cooling strategies on the cooling performance of the power lithium ion battery system: A review,” *Appl. Therm. Eng.*, vol. 142, no. April, pp. 10–29, 2018.

[24] S. J. Drake *et al.*, “Heat generation rate measurement in a Li-ion cell at large C-rates through temperature and heat flux measurements,” *J. Power Sources*, vol. 285, pp. 266–273, Jul. 2015.

[25] J. Smith, R. Singh, M. Hinterberger, and M. Mochizuki, “Battery thermal management system for electric vehicle using heat pipes,” *Int. J. Therm. Sci.*, vol. 134, no. June 2017, pp. 517–529, 2018.

[26] D. Han *et al.*, “Orthogonal experimental design of liquid-cooling structure on

the cooling effect of a liquid-cooled battery thermal management system," *Appl. Therm. Eng.*, vol. 132, pp. 508–520, 2017.

[27] S. Wang, K. Li, Y. Tian, J. Wang, Y. Wu, and S. Ji, "Improved thermal performance of a large laminated lithium-ion power battery by reciprocating air flow," *Appl. Therm. Eng.*, 2019.

[28] A. A. Pesaran, "Battery thermal models for hybrid vehicle simulations," *J. Power Sources*, vol. 110, no. 2, pp. 377–382, Aug. 2002.

[29] S. Guo, R. Xiong, F. Sun, J. Cao, and K. Wang, "An echelon internal heating strategy for lithium-ion battery," *Energy Procedia*, vol. 142, pp. 3135–3140, 2017.

[30] M. Safari, "Battery electric vehicles: Looking behind to move forward," *Energy Policy*, vol. 115, no. January, pp. 54–65, 2018.

[31] A. Mahmoudzadeh Andwari, A. Pesiridis, S. Rajoo, R. Martinez-Botas, and V. Esfahanian, "A review of Battery Electric Vehicle technology and readiness levels," *Renew. Sustain. Energy Rev.*, vol. 78, no. March, pp. 414–430, 2017.

[32] W. Terlouw *et al.*, "Gas for Climate . The optimal role for gas in a net-zero emissions energy system," 2019.

[33] A. A. Pesaran, "Battery Thermal Management in EVs and HEVs : Issues and Solutions," *Adv. Automot. Batter. Conf. Las Vegas, Nevada*, 2011.

[34] M. Khan, M. Swierczynski, S. Kær, M. R. Khan, M. J. Swierczynski, and S. K. Kær, “Towards an Ultimate Battery Thermal Management System: A Review,” *Batteries*, vol. 3, no. 4, p. 9, Mar. 2017.

[35] H. Liu, Z. Wei, W. He, and J. Zhao, “Thermal issues about Li-ion batteries and recent progress in battery thermal management systems: A review,” *Energy Convers. Manag.*, vol. 150, no. May, pp. 304–330, 2017.

[36] Z. Rao and S. Wang, “A review of power battery thermal energy management,” *Renew. Sustain. Energy Rev.*, vol. 15, no. 9, pp. 4554–4571, Dec. 2011.

[37] T. Wang, K. J. Tseng, and J. Zhao, “Development of efficient air-cooling strategies for lithium-ion battery module based on empirical heat source model,” *Appl. Therm. Eng.*, vol. 90, pp. 521–529, 2015.

[38] G.-H. Kim and A. A. Pesaran, “BATTERY THERMAL MANAGEMENT DESIGN MODELING,” *Synapse*, vol. 18, no. 4, pp. 288–293, 1994.

[39] G. Xia, L. Cao, and G. Bi, “A review on battery thermal management in electric vehicle application,” *J. Power Sources*, vol. 367, pp. 90–105, 2017.

[40] R. Zhao, J. Gu, and J. Liu, “Optimization of a phase change material based internal cooling system for cylindrical Li-ion battery pack and a hybrid cooling design,” *Energy*, vol. 135, pp. 811–822, 2017.

[41] W. Li, M. Xiao, X. Peng, A. Garg, and L. Gao, “A surrogate thermal modeling and parametric optimization of battery pack with air cooling for EVs,” *Appl. Therm. Eng.*, vol. 147, no. August 2018, pp. 90–100, 2019.

[42] “Engineered Fluids | AmpCool Dielectric Coolant.” [Online]. Available: https://www.engineeredfluids.com/ampcool. [Accessed: 23-Nov-2018].

[43] “Thermal Management - 3M Novec.” [Online]. Available: https://www.3m.com/3M/en_US/novec-us/applications/thermal-management/. [Accessed: 23-Nov-2018].

[44] “Scopus - Analyze search results | Signed in.” [Online]. Available: https://www.scopus.com/term/analyzer.uri?sid=65d9b5cb806f6d9eaa7a07f7017c4b45&origin=resultslist&src=s&s=%28TITLE-ABS-KEY%28%22Battery+Thermal+Management+Systems%22+OR+%22BTMS%22%29+AND+TITLE-ABS-KEY%28%22Electric+Vehicle%22+OR+%22EV%22%29%29+AND+PUBYEAR+. [Accessed: 21-Jun-2019].

[45] K. Chen, S. Wang, M. Song, and L. Chen, “Configuration optimization of battery pack in parallel air-cooled battery thermal management system using an optimization strategy,” *Appl. Therm. Eng.*, vol. 123, pp. 177–186, Aug. 2017.

[46] W. Li, M. Xiao, X. Peng, A. Garg, and L. Gao, “A surrogate thermal modeling and parametric optimization of battery pack with air cooling for EVs,” *Appl.*

Therm. Eng., vol. 147, no. October 2018, pp. 90–100, 2019.

[47] Z. Liu, Y. Wang, J. Zhang, and Z. Liu, "Shortcut computation for the thermal management of a large air-cooled battery pack," *Appl. Therm. Eng.*, vol. 66, no. 1–2, pp. 445–452, 2014.

[48] Z. Lu *et al.*, "Parametric study of forced air cooling strategy for lithium-ion battery pack with staggered arrangement," *Appl. Therm. Eng.*, vol. 136, no. December 2017, pp. 28–40, 2018.

[49] T. Yang, N. Yang, X. Zhang, and G. Li, "Investigation of the thermal performance of axial-flow air cooling for the lithium-ion battery pack," *Int. J. Therm. Sci.*, vol. 108, pp. 132–144, 2016.

[50] R. Mahamud and C. Park, "Reciprocating air flow for Li-ion battery thermal management to improve temperature uniformity," *J. Power Sources*, vol. 196, no. 13, pp. 5685–5696, 2011.

[51] X. Na, H. Kang, T. Wang, and Y. Wang, "Reverse layered air flow for Li-ion battery thermal management," *Appl. Therm. Eng.*, vol. 143, no. May, pp. 257–262, 2018.

[52] H. Sun and R. Dixon, "Development of cooling strategy for an air cooled lithium-ion battery pack," *J. Power Sources*, vol. 272, pp. 404–414, Dec. 2014.

[53] K. Chen, M. Song, W. Wei, and S. Wang, “Structure optimization of parallel air-cooled battery thermal management system with U-type flow for cooling efficiency improvement,” *Energy*, vol. 145, pp. 603–613, 2018.

[54] K. Chen, M. Song, W. Wei, and S. Wang, “Structure optimization of parallel air-cooled battery thermal management system with U-type flow for cooling efficiency improvement,” *Energy*, vol. 145, pp. 603–613, 2018.

[55] J. Xie, Z. Ge, M. Zang, and S. Wang, “Structural optimization of lithium-ion battery pack with forced air cooling system,” *Appl. Therm. Eng.*, vol. 126, pp. 583–593, 2017.

[56] S. Shahid and M. Agelin-Chaab, “Development and analysis of a technique to improve air-cooling and temperature uniformity in a battery pack for cylindrical batteries,” *Therm. Sci. Eng. Prog.*, vol. 5, no. January, pp. 351–363, 2018.

[57] Z. Lu, X. Z. Meng, L. C. Wei, W. Y. Hu, L. Y. Zhang, and L. W. Jin, “Thermal management of densely-packed EV battery with forced air cooling strategies,” *Energy Procedia*, vol. 88, pp. 682–688, 2016.

[58] S. Hong, X. Zhang, K. Chen, and S. Wang, “Design of flow configuration for parallel air-cooled battery thermal management system with secondary vent,” *Int. J. Heat Mass Transf.*, vol. 116, pp. 1204–1212, 2018.

[59] E. Jiaqiang *et al.*, “Effects of the different air cooling strategies on cooling

performance of a lithium-ion battery module with baffle," *Appl. Therm. Eng.*, vol. 144, no. May, pp. 231–241, 2018.

[60] K. Yu, X. Yang, Y. Cheng, and C. Li, "Thermal analysis and two-directional air flow thermal management for lithium-ion battery pack," *J. Power Sources*, vol. 270, pp. 193–200, 2014.

[61] R. D. Jilte, R. Kumar, and L. Ma, "Thermal performance of a novel confined flow Li-ion battery module," *Appl. Therm. Eng.*, vol. 146, no. September 2018, pp. 1–11, 2019.

[62] F. He, X. Li, and L. Ma, "Combined experimental and numerical study of thermal management of battery module consisting of multiple Li-ion cells," *Int. J. Heat Mass Transf.*, vol. 72, pp. 622–629, May 2014.

[63] Z. Liu, Y. Wang, J. Zhang, and Z. Liu, "Shortcut computation for the thermal management of a large air-cooled battery pack," *Appl. Therm. Eng.*, vol. 66, no. 1–2, pp. 445–452, May 2014.

[64] L. Fan, J. M. Khodadadi, and A. A. Pesaran, "A parametric study on thermal management of an air-cooled lithium-ion battery module for plug-in hybrid electric vehicles," *J. Power Sources*, vol. 238, pp. 301–312, Sep. 2013.

[65] S. Park and D. Jung, "Battery cell arrangement and heat transfer fluid effects on the parasitic power consumption and the cell temperature distribution in a hybrid electric vehicle," *J. Power Sources*, vol. 227, pp. 191–198, Apr. 2013.

[66] D. Jung and D. N. Assanis, “Numerical Modeling of Cross Flow Compact Heat Exchanger with Louvered Fins using Thermal Resistance Concept,” 2006.

[67] G. Y. Cho, J. W. Choi, J. H. Park, and S. W. Cha, “Transient modeling and validation of lithium ion battery pack with air cooled thermal management system for electric vehicles,” *Int. J. Automot. Technol.*, vol. 15, no. 5, pp. 795–803, Aug. 2014.

[68] J. Reyes-Marambio *et al.*, “A fractal time thermal model for predicting the surfacea temperature of air-cooled cylindrical Li-ion cells based on experimental measurements,” *J. Power Sources*, vol. 306, pp. 636–645, Feb. 2016.

[69] E. M. Sparrow, J. P. Abraham, and W. J. Minkowycz, “International Journal of Heat and Mass Transfer Flow separation in a diverging conical duct : Effect of Reynolds number and divergence angle,” *Int. J. Heat Mass Transf.*, vol. 52, no. 13–14, pp. 3079–3083, 2009.

[70] G. G. Lee, W. D. E. Allan, and K. G. Boulama, “International Journal of Heat and Fluid Flow Flow and performance characteristics of an Allison 250 gas turbine S-shaped diffuser : Effects of geometry variations,” *Int. J. Heat Fluid Flow*, vol. 42, pp. 151–163, 2013.

[71] G. G. Lee, W. D. E. Allan, and K. Goni Boulama, “Flow and performance characteristics of an Allison 250 gas turbine S-shaped diffuser: Effects of

geometry variations," *Int. J. Heat Fluid Flow*, vol. 42, pp. 151–163, Aug. 2013.

[72] L. H. Saw, Y. Ye, A. A. O. Tay, W. T. Chong, S. H. Kuan, and M. C. Yew, "Computational fluid dynamic and thermal analysis of Lithium-ion battery pack with air cooling," *Appl. Energy*, vol. 177, pp. 783–792, 2016.

[73] "TÜBİTAK Efficiency Challenge Electric Vehicle." [Online]. Available: https://challenge.tubitak.gov.tr/home_en.html. [Accessed: 21-Aug-2019].

[74] "EVDC - Electric Vehicle Development Center - EMU." [Online]. Available: https://evdc.emu.edu.tr/en. [Accessed: 21-Aug-2019].

[75] Panasonic, "Datasheet : Specifications Powercell NCR18650B," no. 469, p. 1, 2012.

[76] X. Liu, Z. Chen, C. Zhang, and J. Wu, "A novel temperature-compensated model for power Li-ion batteries with dual-particle-filter state of charge estimation," *Appl. Energy*, vol. 123, pp. 263–272, Jun. 2014.

[77] H. Ben Sassi, F. Errahimi, N. Es-Sbai, and C. Alaoui, "IOP Conference Series: Earth and Environmental Science A comparative study of ANN and Kalman Filtering-based observer for SOC estimation Related content A comparative study of ANN and Kalman Filtering-based observer for SOC estimation," vol. 161, p. 12022, 2018.

[78] “View neural network - MATLAB view.” [Online]. Available: https://www.mathworks.com/help/deeplearning/ref/view.html?s_tid=doc_ta. [Accessed: 28-Dec-2019].

[79] X. Qian, D. Xuan, X. Zhao, and Z. Shi, “Heat dissipation optimization of lithium-ion battery pack based on neural networks,” *Appl. Therm. Eng.*, vol. 162, Nov. 2019.

[80] Zhen-Zhe Li, Tai-Hong Cheng, Dong-Ji Xuan, Ming Ren, Gui-Ying Shen, and Yun-De Shen, “Optimal Design for Cooling System of Batteries Using DOE and RSM,” 2012.

[81] “Goodness of Fit Statistics.” [Online]. Available: https://web.maths.unsw.edu.au/~adelle/Garvan/Assays/GoodnessOfFit.html. [Accessed: 01-Jan-2020].

APPENDIX

Table 13: Experiment Results Data Flow

<table>
<tr><th>Input</th><th>Output</th><th colspan="8">Neural Network Training Data</th></tr>
<tr><td rowspan="3">Air Flow rate</td><td></td><td rowspan="3">0.5C</td><td>C_S1_T1</td><td>D_S1_T1</td><td>C_S2_T1</td><td>D_S2_T1</td><td>C_S3_T1</td><td>D_S3_T1</td></tr>
<tr><td rowspan="5">Temperature Profile of 16 Cells per Minute</td><td>C_S1_T2</td><td>D_S1_T2</td><td>C_S2_T2</td><td>D_S2_T2</td><td>C_S3_T2</td><td>D_S3_T2</td></tr>
<tr><td rowspan="2">Current Rate</td><td>C_S1_T3</td><td>D_S1_T3</td><td>C_S2_T3</td><td>D_S2_T3</td><td>C_S3_T3</td><td>D_S3_T3</td></tr>
<tr><td colspan="7"></td></tr>
<tr><td>Parameter</td><td rowspan="3">0.75C</td><td>C_S1_T1</td><td>D_S1_T1</td><td>C_S2_T1</td><td>D_S2_T1</td><td>C_S3_T1</td><td>D_S3_T1</td></tr>
<tr><td rowspan="2">Ambient Temperature</td><td>C_S1_T2</td><td>D_S1_T2</td><td>C_S2_T2</td><td>D_S2_T2</td><td>C_S3_T2</td><td>D_S3_T2</td></tr>
<tr><td>C_S1_T3</td><td>D_S1_T3</td><td>C_S2_T3</td><td>D_S2_T3</td><td>C_S3_T3</td><td>D_S3_T3</td></tr>
<tr><td colspan="2"></td><td colspan="7">Maximum Temperature Analysis per Cell (16)</td></tr>
<tr><td colspan="2" rowspan="4">Output: Average Temperature of cell at each measured instant is done for each C_S1_T(1-3), D_S1_T(1-3) … to D_S3_T(1-3) under both current rate</td><td rowspan="2">0.5C</td><td colspan="2">Charge Speed 1</td><td colspan="2">Charge Speed 2</td><td colspan="2">Charge Speed 3</td></tr>
<tr><td colspan="2">Discharge Speed 1</td><td colspan="2">Discharge Speed 2</td><td colspan="2">Discharge Speed 3</td></tr>
<tr><td colspan="7"></td></tr>
<tr><td rowspan="2">0.75C</td><td colspan="2">Charge Speed 1</td><td colspan="2">Charge Speed 2</td><td colspan="2">Charge Speed 3</td></tr>
<tr><td colspan="2">Discharge Speed 1</td><td colspan="2">Discharge Speed 2</td><td colspan="2">Discharge Speed 3</td></tr>
<tr><td colspan="2"></td><td colspan="7">Maximum Temperature Differences Analysis</td></tr>
<tr><td colspan="2" rowspan="4">Output: Average of Cells 1, 5, 9, 13 into Row1; Cells 2, 6, 10, 14 into Row2; Cells 3, 7, 11, 15 into Row3 and Cells 4, 8, 12, 16 into Row4</td><td rowspan="2">0.5C</td><td colspan="2">Charge Speed 1</td><td colspan="2">Charge Speed 2</td><td colspan="2">Charge Speed 3</td></tr>
<tr><td colspan="2">Discharge Speed 1</td><td colspan="2">Discharge Speed 2</td><td colspan="2">Discharge Speed 3</td></tr>
<tr><td colspan="7"></td></tr>
<tr><td rowspan="2">0.75C</td><td colspan="2">Charge Speed 1</td><td colspan="2">Charge Speed 2</td><td colspan="2">Charge Speed 3</td></tr>
<tr><td colspan="2">Discharge Speed 1</td><td colspan="2">Discharge Speed 2</td><td colspan="2">Discharge Speed 3</td></tr>
<tr><td colspan="2"></td><td colspan="7">Regression Model Training Data</td></tr>
<tr><td>Input</td><td>Output</td><td rowspan="2">0.5C</td><td colspan="2">Charge Speed 1</td><td colspan="2">Charge Speed 2</td><td colspan="2">Charge Speed 3</td></tr>
<tr><td rowspan="2">Air Flow rate</td><td rowspan="3">The Ultimate Maximum Temperature for each Experiment</td><td colspan="2">Discharge Speed 1</td><td colspan="2">Discharge Speed 2</td><td colspan="2">Discharge Speed 3</td></tr>
<tr><td colspan="7"></td></tr>
<tr><td rowspan="2">Current Rate</td><td rowspan="2">0.75C</td><td colspan="2">Charge Speed 1</td><td colspan="2">Charge Speed 2</td><td colspan="2">Charge Speed 3</td></tr>
<tr><td colspan="2">Discharge Speed 1</td><td colspan="2">Discharge Speed 2</td><td colspan="2">Discharge Speed 3</td></tr>
<tr><td colspan="9">Nomenclature</td></tr>
<tr><td colspan="4">C_S1_T1</td><td colspan="5">Charge Experiment_Speed1_Take1</td></tr>
<tr><td colspan="4">D_S2_T3</td><td colspan="5">Discharge Experiment_Speed2_Take3</td></tr>
<tr><td colspan="4">S1, S2, S2</td><td colspan="5">1.4m/s, 2.4m/s, 3.4m/s</td></tr>
<tr><td colspan="4">Take1</td><td colspan="5">First Instant of an Experiment out of 3 Repetition</td></tr>
</table>

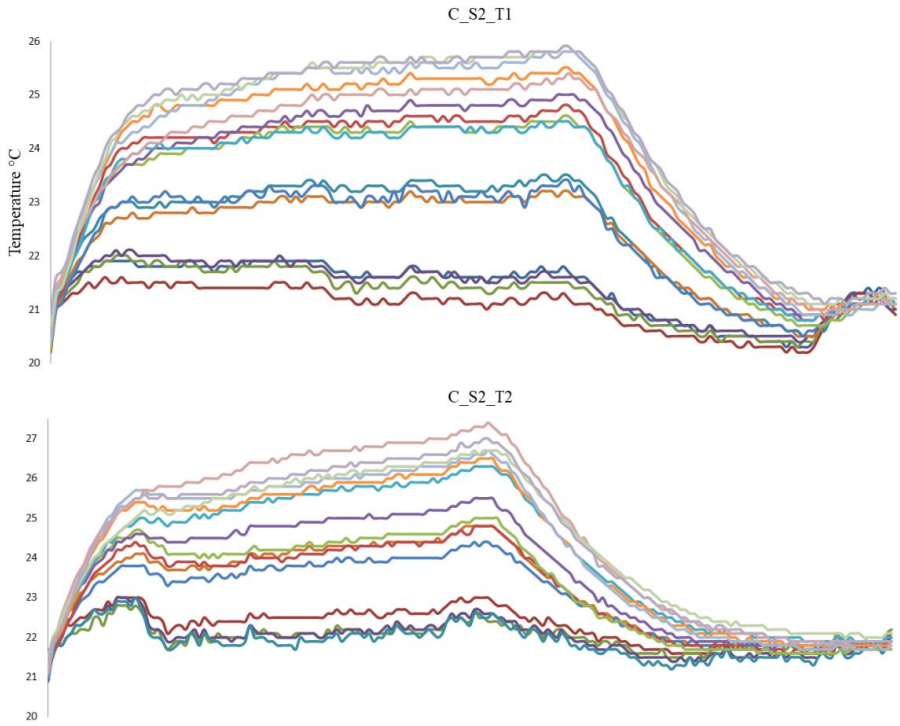

Figure 42: Temperature Profile of Monitored Cells under 0.5C Charge Cycle T1 and T2

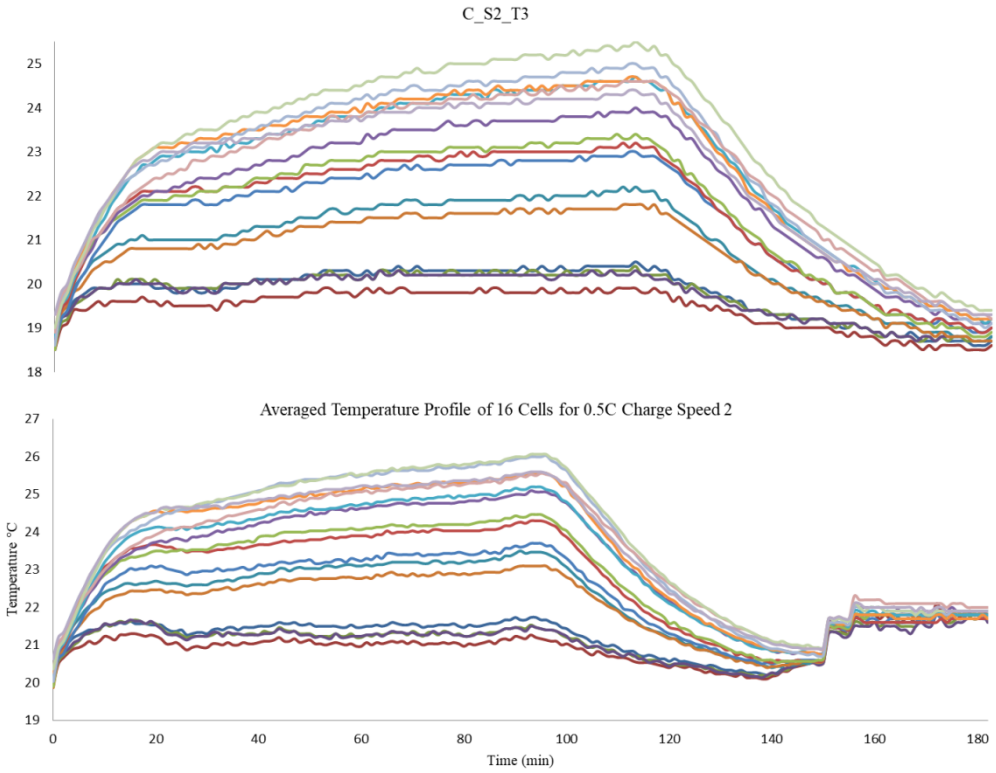

Figure 43: Temperature Profile of Monitored Cells under 0.5C Charge Cycle T3 and Averaged Temperature

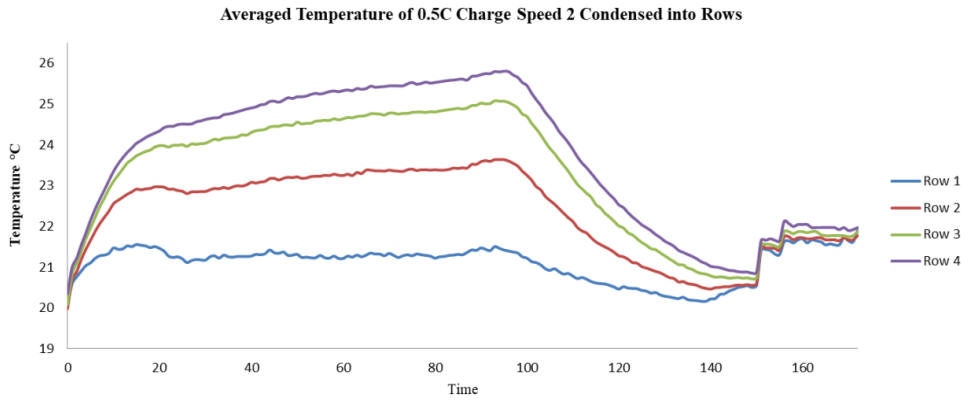

Figure 44: Temperature Profile of Monitored Cells under 0.5C Charge Cycle Converted into Rows of Cells for Temperature Difference Analysis